

Asteria-Pro: Enhancing Deep-Learning Based Binary Code Similarity Detection by Incorporating Domain Knowledge

SHOUGUO YANG, CHAOPENG DONG*, YANG XIAO[†], YIRAN CHENG, ZHIQIANG SHI[‡], ZHI LI, and LIMIN SUN, Institute of Information Engineering, Chinese Academy of Sciences, China and School of Cyber Security, University of Chinese Academy of Sciences, China

The widespread code reuse allows vulnerabilities to proliferate among a vast variety of firmware. There is an urgent need to detect these vulnerable code effectively and efficiently. By measuring code similarities, *AI-based binary code similarity detection* is applied to detecting vulnerable code at scale. Existing studies have proposed various function features to capture the commonality for similarity detection. Nevertheless, the significant code syntactic variability induced by the diversity of IoT hardware architectures diminishes the accuracy of binary code similarity detection. In our earlier study and the tool *Asteria*, we adopt a Tree-LSTM network to summarize function semantics as function commonality and the evaluation result indicates an advanced performance. However, it still has utility concerns due to excessive time costs and inadequate precision while searching for large-scale firmware bugs.

To this end, we propose a novel deep learning enhancement architecture by incorporating domain knowledge-based pre-filtration and re-ranking modules, and we develop a prototype based on *Asteria* called **ASTERIA-PRO**. Pre-filtration module seeks to eliminates dissimilar functions to boost subsequent deep learning model calculations, while re-ranking module aims to raises the rankings of vulnerable functions among candidates generated by deep learning model. Our evaluation indicates that pre-filtration module cuts the calculation time by 96.9% and re-ranking improves MRR and Recall by 23.71% and 36.4%. By incorporating the pre-filtration and re-ranking modules, **ASTERIA-PRO** outperforms existing state-of-the-art approaches in bug search task, by a significant large margin. We conduct a large-scale real-world firmware bug search and **ASTERIA-PRO** manages to detect 1,482 vulnerable functions with a high precision 91.65%.

ACM Reference Format:

Shouguo Yang, Chaopeng Dong, Yang Xiao, YIRAN CHENG, Zhiqiang Shi, Zhi Li, and Limin Sun. 2023. Asteria-Pro: Enhancing Deep-Learning Based Binary Code Similarity Detection by Incorporating Domain Knowledge. 1, 1 (January 2023), 32 pages. <https://doi.org/10.1145/nnnnnnnnnnnnnn>

1 INTRODUCTION

Code reuse is very popular in IoT firmware to facilitate its development [62]. Unfortunately, code reuse also introduces the vulnerabilities concealed in original code to numerous firmware [21]. The security and privacy of our lives are seriously threatened by the widespread use of these firmware [63]. Even though the vulnerabilities have been

* First Author and Second Author contribute equally to this work.

[†] Corresponding author.

[‡] Corresponding author.

Authors' address: Shouguo Yang, yangshouguo@iie.ac.cn; Chaopeng Dong, dongchaopeng@iie.ac.cn; Yang Xiao, xiaoyang@iie.ac.cn; YIRAN CHENG, chengyiran@iie.ac.cn; Zhiqiang Shi, shizhiqiang@iie.ac.cn; Zhi Li, lizhi@iie.ac.cn; Limin Sun, sunlimin@iie.ac.cn, Institute of Information Engineering, Chinese Academy of Sciences, Beijing, China and School of Cyber Security, University of Chinese Academy of Sciences, Beijing, China.

Permission to make digital or hard copies of all or part of this work for personal or classroom use is granted without fee provided that copies are not made or distributed for profit or commercial advantage and that copies bear this notice and the full citation on the first page. Copyrights for components of this work owned by others than ACM must be honored. Abstracting with credit is permitted. To copy otherwise, or republish, to post on servers or to redistribute to lists, requires prior specific permission and/or a fee. Request permissions from permissions@acm.org.

© 2023 Association for Computing Machinery.

Manuscript submitted to ACM

publicly disclosed, there are a large number of firmware that still contain them due to delayed code upgrades or code compatibility issues [17]. Such recurring vulnerabilities, often known as N-day vulnerabilities, cannot be identified by symbol information such as function name because such symbol information is typically stripped during the firmware compilation. Besides, the source code of firmware is not available since IoT vendor only provides binary version of firmware.

To this end, binary code similarity detection (BCSD) is applied to quickly finding homologous vulnerabilities in a large amount of firmware [22]. The BCSD technique focuses on determining the similarity between two binary code pieces. As to the vulnerability search, the BCSD focuses on finding other homologous vulnerable functions given a known vulnerability function. In addition to the vulnerability search, BCSD has been widely used for other security applications such as code plagiarism detection [15, 47, 56], malware detection [41, 42], and patch analysis [27, 33, 61]. Despite many existing research efforts, the diversity of IoT hardware architectures and software platforms poses challenges to BCSD for IoT firmware. There are many different instruction set architectures (ISA) such as ARM, PowerPC, X64, and X86 for IoT firmware. The instructions are different and the rules, such as the calling convention and the stack layout, also differ across different ISAs [54]. It is non-trivial to find homologous vulnerable functions across platforms.

BCSD methods can be generally classified into two categories: i) dynamic analysis-based methods and ii) static analysis-based methods. The methods based on dynamic analysis capture the runtime behavior as function semantic features by running target functions, where the function features can be I/O pairs of function [54] or system calls during the program execution [28], etc. They are not scalable for large-scale firmware analysis since running firmware requires specific devices and emulating firmware is also difficult [19, 34, 70]. The methods based on static analysis mainly extract function features from assembly code. An intuitive way is to calculate the edit distance between assembly code sequences [23]. They cannot be directly applied in cross-architecture since instructions are different across architectures. Architecture-independent statistical features of functions are proposed for the similarity detection [30]. These features are less affected across architectures such as the number of function calls, strings, and constants. Furthermore, the control flow graph (CFG) at the assembly code level is utilized by conducting a graph isomorphism comparison for improving the similarity detection [30, 32]. Based on statistical features and CFG, *Gemini* [64] leverages the graph embedding network to encode functions to vectors for similarity detection. With the application of deep learning models in programming language analysis, various methods have recently appeared to employ such models to encode binary functions in different forms and calculate function similarity based on function encoding [45, 49, 53, 60]. Static analysis-based methods are faster and more scalable for large-scale firmware analysis but often produce false positives due to the lack of semantic information. Since homologous vulnerable functions in different architectures usually share the same semantics, it is desirable that a cross-architecture BCSD can capture the function semantic information in a scalable manner.

In our previous work *Asteria* [68], we first utilize Tree-LSTM network to encode the AST in an effort to fit its semantic representation. In particular, Tree-LSTM is trained using a *siamese* [37] architecture to understand the semantic representation by feeding homologous and non-homologous function pairs into Tree-LSTM network. As a result, the Tree-LSTM network learns function semantic representations to distinguish homologous and non-homologous functions. To further improve the accuracy, we also use the call graph to calibrate the AST similarity. Specifically, we count callee functions of target functions in call graph to measure the function call difference. Final function similarity is determined by calibrating AST similarity with the function call difference. In our previous evaluation, *Asteria* outperforms the available state-of-the-art methods, *Gemini* and *Diaphora* in terms of accuracy. The evaluation results demonstrate the superiority of function semantic extraction by encoding AST with Tree-LSTM model for BCSD.

However, encoding AST incurs a clear temporal cost in *Asteria*. According to our earlier research [68], the entire AST encoding process takes about one second. When *Asteria* is applied to vulnerability detection, where, given a vulnerable function, there are massive functions to do a similarity calculation, the time cost is unacceptable. As the majority of candidate functions are non-homologous, there is space for *Asteria*'s efficiency to be enhanced. In other words, non-homologous candidate functions differ from vulnerable functions in some characteristics that we can exploit to skip most non-homologous functions more efficiently. In addition, vulnerability detection-like evaluation is absent from the majority of efforts [53, 64, 65], including our prior study *Asteria*. It is necessary to evaluate the performance of *Asteria* on the vulnerability search task. Moreover, according to the result in the real world vulnerability detection [68], *Asteria* suffers from high false positives, which affects its effectiveness in reality.

There are two main challenges that hinder *Asteria* from being practical for large-scale vulnerability detection:

- **Challenge 1 (C1).** It's challenging to filter out the majority of non-homologous functions before encoding ASTs, while retaining the homologous ones, to speed up the vulnerability-detection process.
- **Challenge 2 (C2).** It's challenging to distinguish similar but non-homologous functions. Despite *Asteria*'s high precision on homologous and non-homologous classification, it still yields false positives when distinguishing functions with similar ASTs.

We design **ASTERIA-PRO** by introducing domain knowledge with two answers **A1** and **A2** to overcome these two challenges. Our fundamental concept is that introducing inter-functional domain knowledge will help **ASTERIA-PRO** achieve greater precision combined the intra-functional semantic knowledge deep learning model learned. **ASTERIA-PRO** consists of three module: 1) domain knowledge-based (DK-based) pre-filtration, 2) deep learning-based (DL-based) similarity detection, and 3) DK-based re-ranking, among them DL-based similarity detection is basically based on *Asteria*. Domain knowledge is fully exploited for different purpose in DK-based pre-filtration and re-ranking. In pre-filtration module, **ASTERIA-PRO** aims to skip as many as possible non-homologous function by comparing lightweight robust features (**A1**). Meanwhile, the filtration is required to retain all homologous functions. To this end, we conduct a preliminary study into the filtering efficacy of several lightweight function features. According findings of the study, we propose a novel algorithm that successfully employ three distinct function features in the filter. In re-ranking module, **ASTERIA-PRO** confirms the homology of functions by comparing call relationships (**A2**), based on the assumption that functions designed for distinct purposes have different call relationships.

Our evaluation indicates that **ASTERIA-PRO** significantly outperforms existing state-of-the-art methods in terms of both accuracy and efficiency. Compared with *Asteria*, **ASTERIA-PRO** successfully cuts the detection time of **ASTERIA-PRO** by **96.90%** by incorporating DK-based pre-filtration module. By incorporating DK-based re-ranking, **ASTERIA-PRO** manages to enhance the MRR and Recall@Top-1 by 23.71% and 36.4%, to **90.8%** and **89.6%**, respectively. **ASTERIA-PRO** identifies 1,482 vulnerable functions with a high precision of 91.65% by conducting a large-scale real-world firmware vulnerability detection utilizing 90 CVEs. Moreover, the detection results of CVE-2017-13001 demonstrate that **ASTERIA-PRO** has an advanced capacity to detect inlined vulnerable code.

Our contributions are summarized as follows:

- We conduct a preliminary study to demonstrate the effectiveness of various simple function features in identifying non-homologous functions.
- To the best of our knowledge, it is the first work to propose incorporating domain knowledge before and after deep learning models for vulnerability detection optimization. We implement the domain knowledge-based pre-filtration and re-ranking algorithms, and equip them on our previous work.

- The evaluation indicates the pre-filtration significantly reduces the detection time and re-ranking improves the detection precision by a fairly amount. The **ASTERIA-PRO** outperforms existing state-of-the-art methods in terms of both accuracy and efficiency. In evaluation 8.5, we find that the performance of distinct BCSD method may vary widely in different usage scenarios.
- We demonstrate the utility of **ASTERIA-PRO** by conduct a large-scale real-world firmware vulnerability detection. **ASTERIA-PRO** manages to find 1,482 vulnerable functions with a high precision of 91.65%. We analyze the vulnerability distribution in widely-used software of various IoT vendors to illustrates inspiring findings.

2 BACKGROUND

We first briefly describe the AST structure adopted in this work, followed by demonstration of the AST holding more stable structure than CFG across architectures. Then we introduce the Tree-LSTM model utilized in AST encoding. Finally, the broad problem definition for the application of BCSD to bug search is given.

2.1 Abstract Syntax Tree

Table 1. Statements and Expressions in ASTs. We count the statements and expressions for nodes in ASTs after the decompilation by IDA Pro and list the common statements and expressions. This table can be extended if new statements or expressions are introduced.

	Node Type	Label	Note
Statement	if	1	if statement
	block	2	instructions executed sequentially
	for	3	for loop statement
	while	4	while loop statement
	switch	5	switch statement
	return	6	return statement
	goto	7	unconditional jump
	continue	8	continue statement in a loop
	break	9	break statement in a loop
Expression	asgs	10~17	assignments, including assignment, assignment after or, xor, and, add, sub, mul, div
	cmps	18~23	comparisons including equal, not equal, greater than, less than, greater than or equal to, and less than or equal to.
	ariths	24~34	arithmetic operations including or, xor, addition, subtraction, multiplication, division, not, post-increase, post-decrease, pre-increase, and pre-decrease
	other	34~43	others including indexing, variable, number, function call, string, asm, and so on.

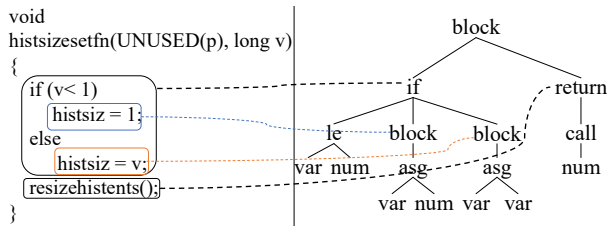


Fig. 1. Source code of function *histsizesetfn* and the corresponding decompiled AST of x86 architecture.

2.1.1 AST Description. An AST is a tree representation of the abstract syntactic structure of code in the compilation and decompilation process. Different subtrees in an AST correspond to different code scopes in the source code. Figure 1 shows a decompiled AST corresponding to the source code of function `histsizesetfn` in zsh v5.6.2 in the left. The zsh is a popular shell software designed for interactive use, and the function `histsizesetfn` sets the value of a parameter. The lines connecting the source code and AST in Figure 1 show that a node in the AST corresponds to an expression or a statement in the source code. A variable or a constant value is represented by a leaf node in AST. We group nodes in an AST into two categories: i) statement nodes and ii) expression nodes according to their functionalities shown in Table 1. Statement nodes control the function execution flow while expression nodes perform various calculations. Statement nodes include `if`, `for`, `while`, `return`, `break` and so on. Expression nodes include common arithmetic operations and bit operations.

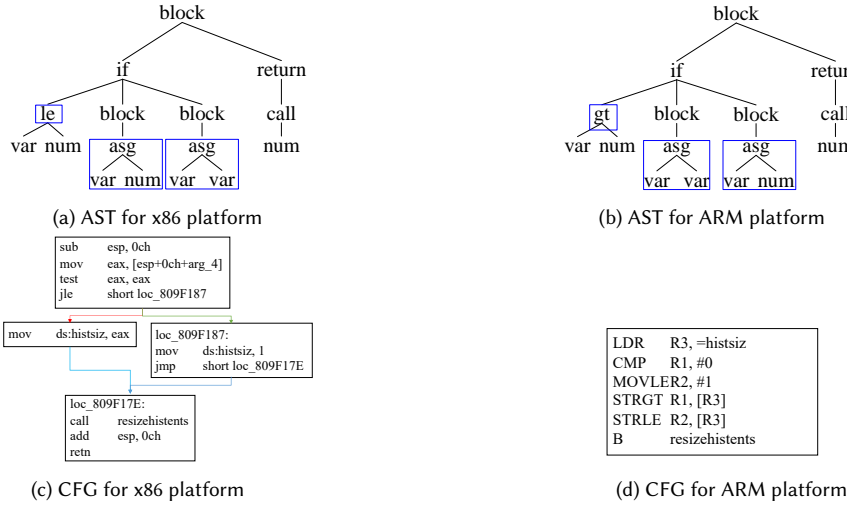


Fig. 2. ASTs and CFGs of the function `histsizesetfn` under different architectures.

2.1.2 AST Structure Superiority. Both CFG and AST are structural representations of a function. The CFG of a function contains the jump relationships between basic blocks that contain straight-line code sequences [38]. Though CFG has been used for similarity measurement in BCSD [30], David *et al.* [23] demonstrated that CFG structures are greatly affected by different architectures. We find AST shows better architectural stability across architectures compared with CFG since the AST is generated from the machine independent intermediate representations which are disassembled from assemble instructions during the decompilation process [20]. Figure 2 shows the changes of ASTs and CFGs in x86 and ARM architectures, respectively. For the CFGs from x86 to ARM, we observe that the number of basic blocks changes from 4 to 1, and the number of assembly instructions has changed a lot. However, the ASTs, based on higher level intermediate representation, slightly change from x86 to ARM, where the changes are highlighted with blue boxes. Besides, AST preserves the semantics of functionality and is thus an ideal structure for cross-platform similarity detection.

2.2 Tree-LSTM Model

In natural language processing, Recursive Neural Networks (RNN) are widely applied and perform better than Convolutional Neural Networks [69]. RNNs take sequences of arbitrary lengths as inputs considering that a sentence can

consist of any number of words. However, standard RNNs are not capable of handling long-term dependencies due to the gradient vanishing and gradient exploding problems. As one of the variants of RNN, Long Short-Term Memory (LSTM) [39] has been proposed to solve such problems. LSTM introduces a gate mechanism including the input, forget, and output gates. The gates control the information transfer to avoid the gradient vanishing and exploding (calculation details in Section § 6.1). Nevertheless, LSTM can only process sequence input but not structured input. Tree-LSTM is proposed to process tree-structured inputs [58]. The calculation by Tree-LSTM model is from the bottom up. For each non-leaf node in the tree, all information from child nodes is gathered and used for the calculation of the current node. In sentiment classification and semantic relatedness tasks, Tree-LSTM performs better than a plain LSTM structure network. There are two types of Tree-LSTM proposed in the work [59]: Child-Sum Tree-LSTM and Binary Tree-LSTM. Researchers have shown that Binary Tree-LSTM performs better than Child-Sum Tree-LSTM [59]. Since the Child-Sum Tree-LSTM does not take into account the order of child nodes, while the order of statements in AST reflects the function semantics, we use the Binary Tree-LSTM for our AST encoding.

3 PRELIMINARY STUDY

This study aims to assess and uncover accessible function features that are effective at identifying non-homologous functions to guide our pre-filtration construction. To evaluate the features, we prepare the code base and incorporate a number of metrics (§ 3.1). To uncover appropriate features, we evaluate and compare popular conventional features found in existing remarkable works (§ 3.2).

3.1 Evaluation Benchmark

3.1.1 Dataset. To derive robust features, we compile a large collection of binaries from 184 open source software (OSS), including widely used OpenSSL, FFmpeg, Binutils, etc. Since our tool aims to conduct similarity detection across different architectures, we compile these OSS to 4 distinct architectures, X86, X64, ARM, and PowerPC. In addition, we align the default compilation settings during compilation with real-world usage. After compilation, numerous test binaries with "test" or "buildtest" as a prefix or suffix are generated to test the software's functionality. These test binaries are removed from the collection because 1) their functions are simple and comprise only a few lines of code. 2) do not participate in the real execution of software function. After removal, the binary collection retains 1,130 binaries, or 226 for each architecture.

We construct a large dataset containing pairs of homologous and non-homologous functions. To this end, function names are retained by software after its compilation. In order to construct homologous function pairs, we utilize binary functions with the same function name in the same software. Otherwise, they form non-homologous functions. For instance, if function F is present in the source code, compilation will generate 4 versions of binary functions for distinct instruction set architectures: F_{x86} , F_{x64} , F_{arm} , and F_{ppc} , respectively. These variants of functions are homologous functions for one another. We extract 132,274 unique binary functions each architecture, for a grand total of 529,096 binary functions. We select at random 40,111 functions from each architecture, totaling 160,444 functions. Among these, we randomly select 1000 functions as source functions and use them to perform filtering operations on all functions. In specifically, source functions are used to evaluate the capability of the target feature to filter away non-homologous functions while preserving homologous ones from the 40,111 functions that have been selected. We prepare the homologous function pairs and groups for feature evaluations. Specifically, we utilize the source function name F together with the library name B , since function names in different binaries might be duplicated but having different functionalities, to combine into a function identifier F^B . After compilation, we will get different homologous

binary functions F_{X86}^B , F_{X64}^B , F_{ARM}^B , and F_{PPC}^B for different architectures, X86, X64, ARM, and PowerPC. These four binary versions of function form a homologous function groups. We pick a random version of function to combine with other 3 versions of functions to form 3 homologous function pairs. We calculate different metrics for function pairs and groups respectively.

3.1.2 Metrics. True positive rate (TPR) and false positive rate (FPR) are utilized to evaluate the filtering capability of various features. TPR demonstrates the feature's capacity to retain homologous functions, while FPR demonstrates its capacity to exclude non-homologous functions. In the subsequent filtering phase, our goal is *to identify features that can filter out non-homologous functions as effectively as possible (low FPR) while maintaining all homologous functions (very high TPR)*.

We employ n source functions to evaluate the filtering capability of diverse features. For each source function F_X^B , we construct a candidate function pool of M randomly selected binary functions, containing three homologous functions of F_X^B . Consequently, source function F_X^B is used to form 3 homologous pairs and $M \times 4 - 4$ non-homologous pairs. The function pair scores are calculated based on distinct feature and scores below a threshold value T are omitted. In the remaining function pairs, the homologous function pair is regarded as a true positive TP while the non-homologous function pair is regarded as a false positive FP . The following equations illustrate how we calculate these three metrics for various features:

$$TPR = \frac{\sum_{i=1}^n TP_i^p}{3 \times n} \quad (1)$$

$$FPR = \frac{\sum_{i=1}^n FP_i}{n \times (M \times 4 - 4)} \quad (2)$$

(3)

3.2 Candidate Features Evaluation

We intend to identify the most efficient and effective filter features by evaluating features proposed in existing studies. On the basis of the evaluation results, we utilize and improve the candidate features for the filter needs.

3.2.1 Feature Selection. We collect basic features from prior research [30, 64, 65, 68] and divide them into two categories: CFG-family feature and AST-family feature. CFG-family features include 5 types of numeric features: *the number of instructions, arithmetic instructions, call instructions, logical instructions, transfer instructions*, and 2 constant features: *string constants and numeric constants* [30]. Since AST must be prepared for model encoding calculation (§ 6), we therefore summarize three syntactic characteristics as AST-family characteristics.

- *No. AST Nodes.* The number of AST nodes.
- *AST node Cluster.* The number of different node types in AST. For example, in Figure 1, the AST node Cluster is denoted as `[block : 3, if : 1, return : 1, call : 1, num : 3, block : 2, asg : 2, var : 4, le : 1]`
- *AST Fuzzy Hash.* We first generate node sequence by traversing the AST preorder. Then we apply the fuzzy hash algorithm [44] to generate the fuzzy hash of AST.

3.2.2 Feature Similarity in Filtration. The format of features divides them into two types with distinct similarity calculations: value type and sequence type. Value type features consist of *No. Instruction, No. Arithmetic, No. Logic, No. Callee, and No. AST nodes*. Sequence type features consist of *Numeric Constant, String Constant, AST Node Cluster, and AST Seq Hash*. For value type features, we use the relative difference ratio (RDR) as shown below for similarity

calculation:

$$RDR(V_1, V_2) = 1 - \frac{abs(V_1 - V_2)}{\max(V_1, V_2)} \quad (4)$$

where V_1, V_2 are feature values. For each sequence-type feature, we first sort the feature's items and then concatenate them into a single sequence. Then, we employ the common sequence ratio (CSR) based on the longest common sequence (LCS) as follows:

$$CSR(S_1, S_2) = \frac{2 \times LCS(S_1, S_2)}{\text{len}(S_1) + \text{len}(S_2)} \quad (5)$$

where S_1, S_2 are feature sequences, and function $LCS(\cdot, \cdot)$ returns the length of the longest common sequence between S_1, S_2 . The above two equations are used for similarity calculation of various features.

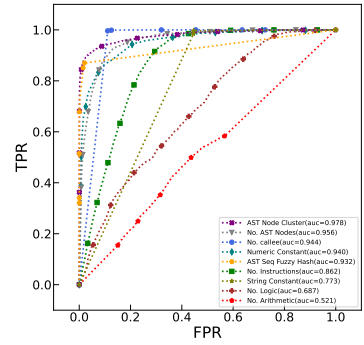


Fig. 3. ROC Curves for Traditional Features.

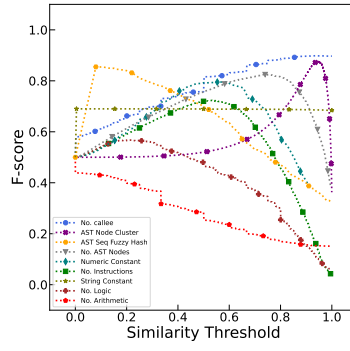


Fig. 4. F_{score} of Traditional Features.

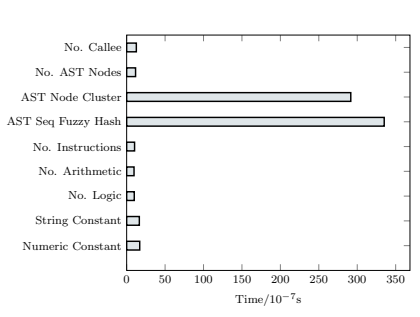


Fig. 5. Time Costs of Similarity Calculation for Different Features.

3.2.3 Evaluation Results. In the evaluation, the values for n and M in § 3.1.2 are set to 1000 and 20,000, respectively. As depicted in Figure 3, TPRs and FPRs calculated for each feature under various thresholds are presented as a receiver operating characteristic (ROC) [71] curve. Additionally, We compute the area under ROC curve (AUC), which reflects the feature's ability to distinguish between homologous and non-homologous functions. The AUC values of the features extracted from AST (i.e., No. AST Nodes, AST Node Cluster, and AST Seq Fuzzy Hash) are high, as presented in the image. However, when the TPR is high, they generate a big FPR. Figure 5 depicts the time costs associated with similarity calculations for various features. Clearly, sequence type features require more time than value type features. Nonetheless, their time consumption falls within an acceptable range of magnitudes. At least 10^5 exact calculations can be completed every second.

We observe in Figure 3 that at high TPR (0.996), the No. Callee feature produces relatively lower FPR (0.111). Recalling the objective of the filtering phase, we aim to select features with a low FPR at a very high TPR. Features with high AUC do not necessarily meet the our objective. For example, the feature AST Node Cluster has a higher FPR (0.47) than feature No. Callee (FPR = 0.111) under the same TPR (0.996), even feature AST Node Cluster has higher AUC (0.978) than feature No. Callee (AUC = 0.944). In this regard, we propose a new metric F_{score} , which indicating high TPR and FPR.

$$F_{score} = \frac{1}{\frac{1}{TPR} + FPR} \quad (6)$$

For each feature, we calculate the F_{score} and plot the F_{score} curves in Figure 4. The Figure 4 plots F_{score} curves of various features at various similarity thresholds. We can see that the No. callee has the best F_{score} (0.90) at threshold

0.94. In this case, we summary the development challenges of *No. callee* and the improvement in § 5 by conducting manually analysis.

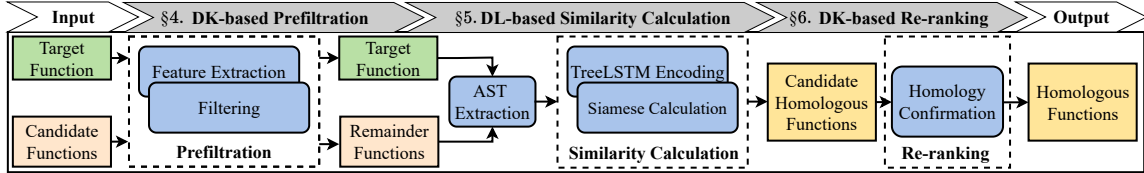


Fig. 6. Workflow of **ASTERIA-PRO**. DK stands for Domain Knowledge. DL stands for Deep Learning.

4 METHODOLOGY OVERVIEW

ASTERIA-PRO consists of three primary modules, **DK-based Prefiltration**, **DL-based Similarity Calculation**, and **DK-based Re-ranking** as shown in Figure 6, where DK stands for Domain Knowledge, and DL stands short for Deep Learning. DK-based prefiltration module utilizes syntactic features to filter out dissimilar functions from candidate functions in a lightweight and efficient manner (see § 5). DL-based similarity calculation module encodes ASTs into representation vectors using the Tree-LSTM model, and determines similarity score between target function and remainder functions using a Siamese network (see § 6). DK-based re-ranking module reorders candidate homologous functions in the above module using lightweight structural features (i.e., function call relationship). **ASTERIA-PRO** can ultimately detect homologous functions across architectures efficiently and effectively.

5 DK-BASED PREFILTRATION

At this stage, **ASTERIA-PRO** intends to incorporate an efficient and effective filter. Callee functions, which are useful in eliminating non-homologous functions demonstrated in preliminary study, are applied extensively for this purpose. We present a variant of the callee function as well as a novel algorithm for constructing the filter.

5.1 Callee Exploitation Challenges

Note that the *No. of callee* only counts the number of callee functions but omits crucial information such as function names. Observing that a portion of callee function names are retained after binary stripping suggests that callee relationship has potential for additional exploration. To fully exploit the callee relationship, we manually analyze the incorrect detection cases of *No. of callee* evaluations in § 3.2 and summarize the challenges to properly exploiting it:

- **Exploitation Challenge 1 (EC1).** Removed or decorated callee function name. For safety and size reasons, the binary usually is stripped after compilation. The call functions whose names are removed after strip from symbol table, can not provide assistance in a straightforward manner. In addition, there are several ways to decorate function names by compiler [9]. The function name will differ from its original name in the source code after decoration.
- **Exploitation Challenge 2 (EC2).** There is no callee functions in some functions (i.e., leaf node in call graph).
- **Exploitation Challenge 3 (EC3).** Function calls in binary target functions might not always be consistent with source code. Function calls may be added or deleted due to compiler optimization. The reasons for the function call change are function inline, intrinsic function replacement, instruction replacement for optimization, that behave differently in different architectures. We describe this challenge in detail in **Function Call Optimization**.

To overcome exploitation challenges, we design a new feature **genealogist** derived from callee relationship. The novel algorithm **UpRelation** is proposed to exploit the new feature.

5.2 Filter Feature Design

Our new feature intends to extract comprehensive information from the call relationship of software binary, including the symbol information. Such call relationship can be presented by *call graph*. The *call graph* CG can be defined by giving all functions as nodes and the call relationships between functions as edges: $CG = (\mathcal{V}, \mathcal{E})$, where $\mathcal{V} = \{v | v \text{ is a function}\}$ denotes the node collection and $\mathcal{E} = \{(u, v) | u \text{ calls } v\}$ denotes the edge collection. For edge $(u, v) \in E$, we say that function v is a callee function of function u . The genealogist is a function list containing **partial** callee functions of the target function. Considering **EC1**, we can not utilize all symbol information of callee functions, since callee functions might be in removable symbol table (i.e., static symbol table), and the function name will be removed. Fortunately, to link against dynamic libraries, function names in the dynamic symbol table DST (i.e., import and export table) will be preserved [36]. For example, if target function calls external function ‘`strcpy`’, the callee function name ‘`strcpy`’ remains in import table rather than removed after binary strip. We define genealogist GL of target function f as: $GL_f = \{v | v \in \mathcal{V}, (f, v) \in \mathcal{E}, v \in DST\}$.

For cases where a function calls the same function multiple times, we keep multiple identical function names.

5.3 Filtration algorithm

To support our new feature, we propose a feature similarity algorithm, called **UpRelation**. The algorithm utilizes context information in the call graph to overcome challenge **EC2**, **EC3**. Specifically, the algorithm utilizes parent nodes of leaf nodes in call graph to match leaf nodes to address the **EC2**. In the algorithm, we adopt a drill down strategy, that combines three feature GL , *No. Callee*, and *String Constants* according to their information content, considering the fairly robust performance of *No. Callee* and *String Constants* in preliminary evaluation. The *No. Callee* of function f is denoted by $Callee_f$ and the *String Constant* set of function f is denoted by $StrCons_f$.

Given a vulnerable function f_v , Algorithm 1 aims to omit the most of non-homologous functions, with retaining vulnerable candidate function to a list (VFL) from target function list TFL . Code from line 2 to line 6 performs filtering when feature genealogist GL_{f_v} of f_v is not empty. Specifically, the algorithm calculates the *CSR* between GL_{f_v} and GL_f of all candidate functions in line 4. Then it filters out functions whose *CSR* is less than a threshold T_{GL} . Similarly, when callee number $Callee_{f_v}$ of f_v is not 0, it filters out functions by calculating *RDR* score from line 7 to line 11. Line 12 to 19 makes up the most crucial portion of the algorithm, which matches the leaf functions to address **EC2**. All caller functions of f_v are first visited in this section of the algorithm at line 14. It employs *UpRelation* to discover all functions that are similar to caller function, fp . For each similar function fp' , the algorithm regards all its callee functions as vulnerable candidate functions at line 16. We find the same leaf functions by locating the same caller functions because the caller functions of the same leaf functions are also the same. However, this introduces some extraneous (leaf) functions, that share the same caller function but are not the same as the leaf function. We utilize string similarity at line 22, to remove extraneous functions. After filtering by callees and strings, the algorithm finally gets the expected vulnerable candidate function list VFL .

6 DL-BASED SIMILARITY CALCULATION

This module calculates the similarity between two function ASTs by encoding them into vectors and applying the Siamese architecture to calculate similarity between encoded vectors. Figure 7 depicts the calculation flow.

Algorithm 1: UpRelation

Input: Vulnerable Function fv , Target Function List TFL , Thresholds $T_{GL}, T_{callee}, T_{string}$
Output: Vulnerable Candidate Function List VFL

```

1  $VFL \leftarrow TFL;$ 
2 if  $GL_{fv}$  is not null then
3   for  $f \in TFL$  do
4      $s = CSR(GL_{fv}, GL_f);$ 
5     if  $s < T_{GL}$  then  $VFL.pop(f);$ 
6   end
7 else if  $Callee_{fv} > 0$  then
8   for  $f \in TFL$  do
9      $s = RDR(Callee_{fv}, Callee_f);$ 
10    if  $s < T_{callee}$  then  $VFL.pop(f);$ 
11   end
12 else
13    $FL' = \emptyset;$ 
14   for  $fp \in GetCallers(fv)$  do
15     for  $fp' \in UpRelation(fp, VFL)$  do
16        $FL'.add(GetCallees(fp'));$ 
17     end
18   end
19    $VFL = FL';$ 
20 if  $StrCons_{fv}$  is not null then
21   for  $f \in VFL$  do
22      $s = CSR(StrCons_{fv}, StrCons_f);$ 
23     if  $s < T_{string}$  then  $VFL.pop(f);$ 
24   end
25 else
26   return
27 end
28  $VFL;$ 

```

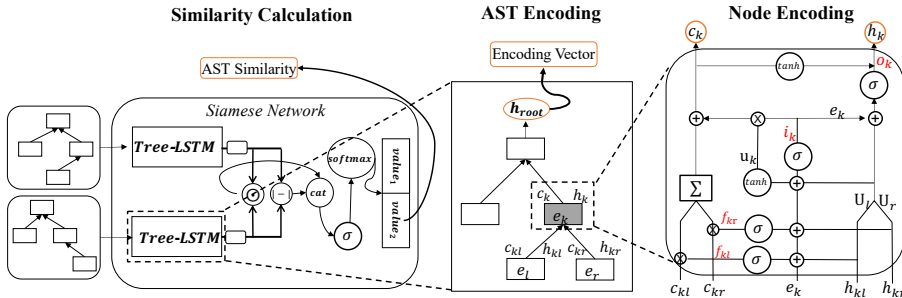


Fig. 7. The Siamese Architecture and Tree-LSTM Encoding.

6.1 Tree-LSTM Encoding

Given an AST, Tree-LSTM model encodes it into a representation vector. Tree-LSTM model is firstly proposed to encode the tree representation of a sentence and summarize the semantic information in natural language processing. Tree-LSTM model can preserve every property of the plain LSTM gating mechanisms while processing tree-structured inputs. The main difference between the plain LSTM and the Tree-LSTM is the way to deal with the outputs of predecessors. The plain LSTM utilizes the output of only one predecessor in the sequence input. We utilize Tree-LSTM to integrate the outputs of all child nodes in the AST for calculation of the current node. To facilitate the depiction of the Tree-LSTM encoding, we assume that node v_k has two child nodes v_l and v_r . The Tree-LSTM encoding of node v_k takes three types of inputs: node embedding e_k of v_k , hidden states h_{kl} and h_{kr} , and cell states c_{kl} and c_{kr} as illustrated in Figure 7. The node embedding e_k is generated by using the pre-trained model CodeT5 to embed the node v_k to a high-dimensional representation vector. h_{kl} , h_{kr} , c_{kl} , and c_{kr} are outputs from the encoding of child nodes. During the node encoding in Tree-LSTM, there are three gates and three states which are important in the calculation. The three gates are calculated for filtering information to avoid gradient explosion and gradient vanishing [58]. They are input, output, and forget gates. There are two forget gates f_{kl} and f_{kr} , filtering the cell states from the left child node and right child node separately. As shown in **Node Encoding** in Figure 7, the forget gates are calculated by combining h_{kl} , h_{kr} , and e_k . Similar to the forget gates, the input gate, and the output gate are also calculated by combining h_{kl} , h_{kr} , and e_k . The details of the three types of gates are as follows:

$$f_{kl} = \sigma(W^f e_k + (U_{ll}^f h_{kl} + U_{lr}^f h_{kr}) + b^f) \quad (7)$$

$$f_{kr} = \sigma(W^f e_k + (U_{rl}^f h_{kl} + U_{rr}^f h_{kr}) + b^f) \quad (8)$$

$$i_k = \sigma(W^i e_k + (U_l^i h_{kl} + U_r^i h_{kr}) + b^i) \quad (9)$$

$$o_k = \sigma(W^o e_k + (U_l^o h_{kl} + U_r^o h_{kr}) + b^o) \quad (10)$$

where i_k and o_k denote the input gate and the output gate respectively, and the symbol σ denotes the sigmoid activation function. The weight matrix W , U , and bias b are different corresponding to different gates. After the gates are calculated, there are three states u_k , c_k , and h_k in Tree-LSTM to store the intermediate encodings calculated based on inputs h_{kl} , h_{kr} , and e_k . The cached state u_k combines the information from the node embedding e_k and the hidden states h_{kl} and h_{kr} (Equation 11). And note that u_k utilizes \tanh as the activation function rather than *sigmoid* for holding more information from the inputs. The cell state c_k combines the information from the cached state u_k and the cell states c_{kl} and c_{kr} filtered by forget gates (Equation 12). The hidden state h_k is calculated by combining the information from cell state c_k and the output gate o_k (Equation 13). The three states are computed as follows:

$$u_k = \tanh(W^u e_k + (U_l^u h_{kl} + U_r^u h_{kr}) + b^u) \quad (11)$$

$$c_k = i_k \odot u_k + (c_{kl} \odot f_{kl} + c_{kr} \odot f_{kr}) \quad (12)$$

$$h_k = o_k \odot \tanh(c_k) \quad (13)$$

where the \odot means Hadamard product [40]. After the hidden state and input state are calculated, the encoding of the current node v_k is finished. The states c_k and h_k will then be used for the encoding of v_k 's parent node. During the AST encoding, Tree-LSTM encodes every node in the AST from bottom up as shown in **Tree-LSTM Encoding** in Figure 7. After encoding all nodes in the AST, the hidden state of the root node is used as the encoding of the AST.

6.2 Siamese Calculation

This step uses Siamese architecture that integrates two identical Tree-LSTM model to calculate similarity between encoded vectors. The details of the Siamese architecture $\mathcal{M}(T_1, T_2)$ are shown in Figure 7. The Siamese architecture consists of two identical Tree-LSTM networks that share the same parameters. In the process of similarity calculation, the Siamese architecture first utilizes Tree-LSTM to encode ASTs into vectors. We design the Siamese architecture with subtraction and multiplication operations to capture the relationship between the two encoding vectors. After the operations, the two resulting vectors are concatenated into a larger vector. Then the resulting vector goes through a layer of *softmax* function to generate a 2-dimensional vector. The calculation is defined as:

$$\mathcal{M}(T_1, T_2) = \text{softmax}(\sigma(\text{cat}(|\mathcal{N}(T_1) - \mathcal{N}(T_2)|, \mathcal{N}(T_1) \odot \mathcal{N}(T_2)) \times W)) \quad (14)$$

where W is a $2n \times 2$ matrix, the \odot represents Hadamard product [40], $|\cdot|$ denotes the operation of making an absolute value, the function $\text{cat}(\cdot)$ denotes the operation of concatenating vectors. The softmax function normalizes the vector into a probability distribution. Since W is a $2n \times 2$ weight matrix, the output of Siamese architecture is a 2×1 vector. The format of output is $[\text{dissimilarity score}, \text{similarity score}]$, where the first value represents the dissimilarity score and the second represents the similarity score. During the model training, the input format of Siamese architecture is $\langle T_1, T_2, \text{label} \rangle$. In our work, the label vector $[1, 0]$ means T_1 and T_2 are from non-homologous function pairs and the vector $[0, 1]$ means homologous. The resulting vector and the label vector are used for model loss and gradient calculation. During model inference, the second value in the output vector is taken as the similarity of the two ASTs, and the similarity of ASTs is used in re-ranking.

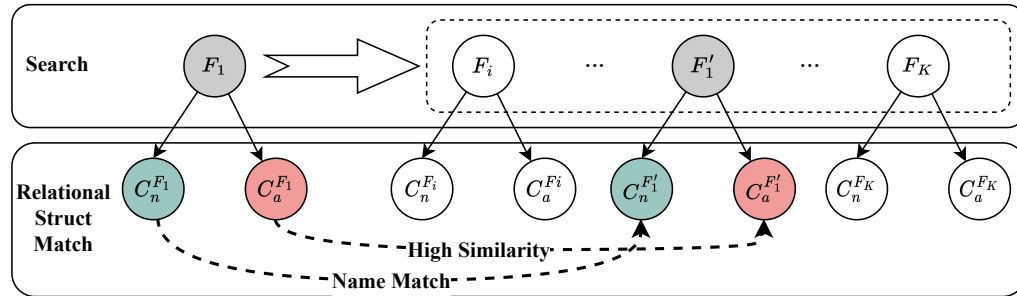


Fig. 8. The Re-ranking Motivation Example. In the rectangular box with dashed line are the top K candidate homologous functions of F_1 produced by the search (i.e., DL-based similarity detection). Solid line arrows indicate the function call relationship (e.g., F_1 calls $C_n^{F_1}$). The dotted line arrows indicate the callee function match in re-ranking.

7 DK-BASED RE-RANKING

This module seeks to confirm the homology of top k candidate functions output by Tree-LSTM network by re-ranking them. In the prior phase, the Tree-LSTM network infers the semantic information from AST, which is a intra-functional feature. The knowledge gained from AST is insufficient for establishing the homology of functions. In this phase, function call relationships are used as domain knowledge to compensate for the lack of knowledge regarding the inter-functional features of the Tree-LSTM. To this end, we design an algorithm called **Relational Structure Match**. In contrast to the callee application in the pre-filtering module, this module uses more extensive information from calle relationships, to show degree of homology of candidate functions.

7.1 Motivated Example

Our algorithm is based on a conforming observation to an intuitive law: *If a function F_1 calls function C^{F_1} , then its homologous function F'_1 will also call the homologous function $C^{F'_1}$ of C^{F_1} .* As depicted in Figure 8, we have F_1 calls C^{F_1} , and F'_1 calls $C^{F'_1}$. Assume that the search process for F_1 yields top K functions containing the target homologous function F'_1 . We then employ the call relations of F_1 and F'_1 to conduct precise callee function match for re-ranking. In particular, callee functions of F_1 are divided into two categories, named callees $C_n^{F_1}$ and anonymous callees $C_a^{F_1}$. For named callees, their names are utilized to match callees of functions between source function F_1 and candidate top K functions. For anonymous callees, we employ DL-based similarity detection to calculate similarity between callees of functions between source function F_1 and candidate top K functions. Recall the observation, the homologous function F'_1 of F_1 holds the most matched callees. F'_1 is re-ranked in first place after candidate functions are re-ranked based on matched callees.

7.2 Relational Structure Match Algorithm

This algorithm aims to rescore each candidate function by fully exploiting the call relationship of target function and candidate functions. The relational structure refers to call relations between target function and all its callee functions as illustrated in Section § 7.1. To match relational structure, given a source function F_1 , the algorithm executes one of following two distinct operations (O_1 and O_2) based on whether the source function has callee functions or not.

- O_1 : When F_1 has callee function(s), the algorithm extracts all callee functions of F_1 to build *mixed callee function set* (MCFS) (described below). Based on MCFS, the algorithm detects similarities between the target functions and candidate functions as new scores. It re-ranks all candidate functions by combining the **Asteria** scores (Equation 6) with the newly calculated match scores. The details of MCFS and match score calculation are described below.
- O_2 : When F has no callee function, the algorithm removes all candidate functions which have callee function(s). Then the left candidate function are re-ranked by their **Asteria** scores.

Mixed Callee Function Set. The *mixed callee function set* of function F is comprised of two types of callee functions: named callee and anonymous callee. Anonymous callee refers to a type function for which the function name has been removed for security reasons. The other type of callee functions have their names preserved because they are imported or exported functions and the function name is necessary for external link purpose. These callee functions are called named callee. We denote MCFS of F with $CS_F = \{C_{n1}^F, \dots, C_{nj}^F, C_{a1}^F, \dots, C_{aj}^F\}$, where C_{nj}^F denotes named callee function and C_{aj}^F denotes anonymous callee function.

Match Score Calculation. With MCFSs of target function F_1 and all candidate functions extracted, the algorithm conducts two kinds of matches between callees to calculate match score M for each candidate function.

- Named Callee Match.* For all named callees $C_n^{F_1}$ in CS_{F_1} , the algorithm matches them and named callees of each candidate functions by function name. For example, the named callee $C_n^{F_1}$ and $C_n^{F'_1}$ share the same function name in Figure 8 so they are matched. The number of matched functions of candidate function F_i is denoted as $N_n^{F_i}$.
- Anonymous Callee Match.* For all anonymous callee $C_{ai}^{F_1}$ in CS_{F_1} , the algorithm utilizes DL-based similarity detection to calculate similarity scores between all anonymous callees of all candidate functions. For each anonymous callee $C_{aj}^{F_i}$ in candidate function F_i , the algorithm takes the maximum similarity score between it and all anonymous callees of target function as its score $S_{aj}^{F_i}$.

After matching all callee functions of candidate functions, for candidate function F_i , the match score M_{F_i} of F_i is calculated as follows:

$$M_{F_i} = \mathcal{N}_n^{F_i} + \sum \mathcal{S}_{aj}^{F_i} \quad (15)$$

where $\mathcal{S}_{aj}^{F_i} \in CS_{F_i}$.

Match Score-based Re-ranking. The re-ranking score of candidate function F_i is combined by match score M_{F_i} and its DL-based similarity $\mathcal{M}_{\mathcal{F}_i}$ in Equation 14. We calculate new score $S_{F_i}^{re-rank}$ for all candidate functions with following equation:

$$S_{F_i}^{re-rank} = \alpha \times \mathcal{M}_{\mathcal{F}_i} + \beta \times M_{F_i} \quad (16)$$

where $\alpha + \beta = 1$. All candidate functions are resorted by their new rank scores $S_{F_i}^{re-rank}$ in descending order.

8 EVALUATION

We aim to conduct a comprehensive practicality evaluation of various state-of-the-art function similarity detection methods for bug search. To this end, we adopt 8 different metrics to depict the search capability of different methods in a more comprehensive way. Furthermore, we construct a large evaluation dataset, in a way that is closer to practical usage of function similarity detection.

8.1 Research Questions

In the evaluation experiments, we aim to answer following research questions:

- RQ1.** How does **ASTERIA-PRO** compare to baseline methods in cross-architecture function similarity detection on the two detection tasks?
- RQ2.** What is the performance of **ASTERIA-PRO**, compared to baseline methods in Task-V?
- RQ3.** How much do DK-based filtration and DK-based re-ranking improves in accuracy and efficiency?
- RQ4.** How does **ASTERIA-PRO** perform in real-world bug search?

8.2 Implementation Details

We utilize IDA Pro 7.5 [4] and its plug-in *Hexray Decompiler* to decompile binary code for AST extraction. This version of *Hexray Decompiler* currently supports the architectures of x86, x64, PowerPC (PPC), and ARM. We use the *Hexray Decompiler* to decompile the target binaries and extract the ASTs. For the encoding of leaf nodes in Formulas (7)-(12), we assign the state vectors h_{kl} , h_{kr} , c_{kl} , and c_{kr} to zero vectors. The loss function for model training is *BCELoss*, which measures the binary cross entropy between the labels and the predictions. The *AdaGrad* optimizer is applied for gradient computation and weight-matrix updating after losses are computed. Since the computation steps of Tree-LSTM depend on the shape of the AST, therefore, we cannot perform parallel batch computation, which makes the batch size always to be 1. The model is trained for 60 epochs. Our experiments are performed on a local server equipped with two Intel(R) Xeon(R) CPUs E5-2620 v4 @ 2.10GHz, each with 16 cores, 128GB of RAM, and 4T of storage. The code of **ASTERIA-PRO** runs in a Python 3.6 environment. We use `gcc v5.4.0` compiler to compile source code in our dataset, and use the `buildroot-2018.11.1` [1] for the dataset construction. We use the tool `binwalk` [5] to unpack the firmware for obtaining the binaries to conduct further analysis. In **UpRelation** algorithm of filtering module, we set values of thresholds T_{GL} , T_{callee} , T_{string} to 0.1, 0.8, 0.8 based on their F_{score} , respectively. The crucial threshold T_{GL}

is discussed in § 8.7.1. We merely set $\alpha = 0.1, \beta = 0.9$ in Equation 16 to emphasize role of callee function similarities in re-ranking.

8.3 Comprehensive Benchmark

To compare BCSD methods in a comprehensive way, we build an extensive benchmark based on multiple advanced works [50, 60, 64]. The benchmark comprises of two datasets, two detection tasks, and six measure metrics, where two datasets are utilized separately for each of the two detection tasks.

8.3.1 Dataset. The functions not involved in the prefiltering test (see § 3) are divided into two datasets for model training and testing and evaluation.

Model Dataset Construction. We select 31,940 functions from 1944 distinct binaries to construct 314,852 homologous function pairs and 314,852 non-homologous function pairs, respectively. Then, we divided all function pairs by an 8:2 ratio into training set and testing set. This dataset is constructed for Tree-LSTM training and testing.

Evaluation Dataset Construction. We randomly select 60,221 functions from each architecture’s 2,875 binaries. Using these functions, two sub-datasets for two evaluation tasks are constructed. The first sub-dataset is constructed in a classification manner for technique comparison [64, 65], and the second sub-dataset is constructed in a bug search manner. Each dataset includes a large number of *to-be-matched* tuples, each of which is in form of (F, P_{set}) , where P_{set} denotes a function set containing candidate functions to be matched with source function F . Given a source function F , the first sub-dataset combines one of its homologous function F_h and a non-homologous function F_n as P_{set} . To emulate the bug search, the second sub-dataset puts more non-homologous functions into the P_{set} . Specifically, given a source function F , we randomly choose a homologous function and pick N non-homologous functions into the P_{set} . We call the first sub-dataset **g-dataset** and the second sub-dataset **v-dataset**. In v-dataset, we randomly pick 10,000 non-homologous functions for the P_{set} . The formal representation of two datasets are as following:

$$\text{g-dataset} : \{(F, (F_h, F_n)), \} \quad (17)$$

$$\text{v-dataset} : \{(F, (F_h, F_{n1}, \dots, F_{ni}, \dots, F_{n10000})), \} \quad (18)$$

where F_h denotes the homologous functions, and F_{ni} denotes the i th non-homologous function. For each dataset, the source function F will be matched with all functions in the P_{set} for evaluation.

8.3.2 Metrics. We choose five distinct metrics for comprehensive evaluation from earlier works [53, 60, 68]. In our evaluation, the similarity of a function pair is calculated as a score of r . Assuming the threshold is β , if the similarity score r of a function pair is greater than or equal to β , the function pair is regarded as a positive result, otherwise a negative result. For a homologous pair, if its similarity score r is greater than or equal to β , it is a true positive (**TP**). If a similarity score of r is less than β , the calculation result is a false negative (**FN**). For a non-homologous pair, if a similarity score r is greater than or equal to β , it is a false positive (**FP**). When the similarity score r is less than β , it is a true negative (**TN**). These metrics are described as following:

- **TPR.** TPR is short for true positive rate. TPR shows the accuracy of homologous function detection at threshold β . It is calculated as $TPR = \frac{TP}{TP+FN}$.
- **FPR.** FPR is short for false positive rate. FPR shows the accuracy of non-homologous function detection at threshold β . It is calculated as $FPR = \frac{FP}{FP+TN}$.

- **AUC.** AUC is short for area under the curve, where the curve is termed Receiver Operating Characteristic (**ROC**) curve. The ROC curve illustrates the detection capacity of both homologous and non-homologous functions as its discrimination threshold β is varied. AUC is a quantitative representation of ROC.
- **MRR.** MRR is short for mean reciprocal rank, which is a statistic measure for evaluating the results of a sample of queries, ordered by probability of correctness. It is commonly used in retrieval experiments. In our evaluation, it is calculated as $MRR = \frac{1}{|P_{set}|} \sum_{F_{hi} \in P_{set}} \frac{1}{Rank_{F_{hi}}}$, where $Rank_{F_{hi}}$ denotes the rank of function F_{hi} in pairing candidate set P_{set} , and $|P_{set}|$ denotes the size of P_{set} .
- **Recall@Top-k.** It shows the capacity of homologous function retrieve at top k detection results. The top k results are regarded as homologous functions (positive). It is calculated as follows:

$$g(x) = \begin{cases} 1 & \text{if } x = \text{True} \\ 0 & \text{if } x = \text{False} \end{cases}$$

$$Recall@k = \frac{1}{|F|} \sum g(Rank_{f_i^{gt}} \leq k)$$

To demonstrate the reliability of the ranking results, we adopt Recall@Top-1 and Recall@Top-10.

8.3.3 *Detection Tasks.* We present the following two function similarity detection tasks based on BCSD applications [35]:

- **C-task.** C-task stands for classification task. This task aims to test the ability of the methods to discriminate between homologous and non-homologous functions. C-task performs binary classification for homologous and non-homologous functions on dataset **g-dataset** and calculates three metrics: TPR, FPR, AUC, since they are generally used to indicate the binary classification performance of the model. The **g-dataset** meets the dataset requirement and is used in this task.
- **V-task.** V-task stands for bug (vulnerability) search task. This task aims to evaluate the capacity of identifying vulnerable functions from a vast pool of candidate functions. In other words, given a source function, it is the same action to find its homologous function from candidate functions. This data requirement is met by the **v-dataset**. More specifically, for a *to-be-matched* tuple (F, P_{set}) , tested methods calculate function similarity between source function F and all functions in P_{set} . After similarity calculation, the functions in the P_{set} can be sorted by similarity scores. Metrics MRR, Recall@Top-1, and Recall@Top-10 are calculated in this task.

8.4 Baseline Methods.

We choose various representative cross-architectural BCSD works, that make use of AST or are built around deep learning encoding. These BCSD works consist of *Diaphora* [2], *Gemini* [64], *SAFE* [51], and *Trex* [53]. Moreover, we also use our previous conference work *Asteria* as one of baseline methods. We go over these works in more details below.

Diaphora. *Diaphora* performs similarity detection also based on AST. *Diaphora* maps nodes in an AST to primes and calculates the product of all prime numbers. Then it utilizes a *difference function* to calculate the similarity between the prime products. We download the *Diaphora* source code from github [2], and extract *Diaphora*'s core algorithm for AST similarity calculation for comparison. Noting that it would take a significant amount of time (several minutes) to compute a pair of functions with extremely dissimilar ASTs, we add a filtering computation before the prime difference. The filtering calculates the AST size difference and eliminates function pairs with a significant size difference. We publish the improved *Diaphora* source code on our website [6].

Table 2. AUCs in Task-C.

Methods	X86-ARM	X86-X64	X86-PPC	ARM-X64	ARM-PPC	X64-PPC	Average
Asteria	0.995	0.998	0.998	0.995	0.998	0.999	0.997
Gemini	0.969	0.984	0.984	0.973	0.968	0.984	0.977
SAFE	0.851	0.867	-	0.872	-	-	0.863
Trex	0.794	0.891	-	0.861	-	-	0.849
Diaphora	0.389	0.461	0.397	0.388	0.455	0.400	0.415

Gemini. *Gemini* encodes ACFGs (attributed CFGs) into vectors with a graph embedding neural network. The ACFG is a graph structure where each node is a vector corresponding to a basic block. We have obtained *Gemini*'s source code and its training dataset. Notice that in [64] authors mentioned it can be retrained for a specific task, such as the bug search. To obtain the best accuracy of *Gemini*, we first use the given training dataset to train the model to achieve the best performance. Then we re-train the model with the part of our training dataset. *Gemini* supports similarity detection on X86, MIPS, and ARM architectures.

SAFE. *SAFE* works directly on disassembled binary functions, does not require manual feature extraction, is computationally more efficient than *Gemini*. In their vulnerability search task, *SAFE* outperforms *Gemini* in terms of recall. *SAFE* supports three different instruction set architecture X64, X86, and ARM. We retrain *SAFE* based on the official code [51] and use retrained model parameter for our test. In particular, we select all appropriate function pairs from the training dataset, whose instruction set architectures are supported by *SAFE*. Then we extract the function features for all function pairs selected and discard the function pairs whose features *SAFE* cannot extract. After feature extraction, 27,580 function pairs of three distinct architecture combinations (i.e., X86-X64, X86-ARM, and X64-ARM) are obtained for training. Next, We adopt the default model parameters (e.g., embedding size) and training setting (e.g. training epoches) to train *SAFE*.

Trex. *Trex* is based on pretrained model [53] of the state-of-the-art NLP technique, and micro-traces. It utilizes a dynamic component to extract micro-traces and use them to pretrain a masked language model. Then it integrates pretrained ML model into a similarity detection model along with the learned semantic knowledge from micro-traces. It supports similarity detection of ARM, MIPS, X86, and X64.

8.5 Comparison of Cross-architecture Similarity Detection (RQ1)

We evaluate various approaches on two distinct tasks. Due to the fact that the baseline methods may not be able to detect for all four instruction set architectures, the detection results for some architecture combinations are empty. In the two paragraphs that follow, the outcomes of two distinct tasks are discussed.

Comparison on task-C. For task-C, we evaluate all approaches by performing similarity detection on all supported architectural combinations. After detection, the three task-C-referenced metrics are calculated and presented in Table 2 and Figure 9. In each subplot of Figure 9, the x-axis represents FPR, while the y-axis represents TPR. Six subplots depict the ROC curves of various architecture combinations. In general, methods with performance curves closer to the upper-left corner have a superior performance. It is evident from all subplots that our model outperforms all baseline methods. Quantitatively, the AUC values of our model are greater than those of the other baseline techniques for any architectural combination in Table 2.

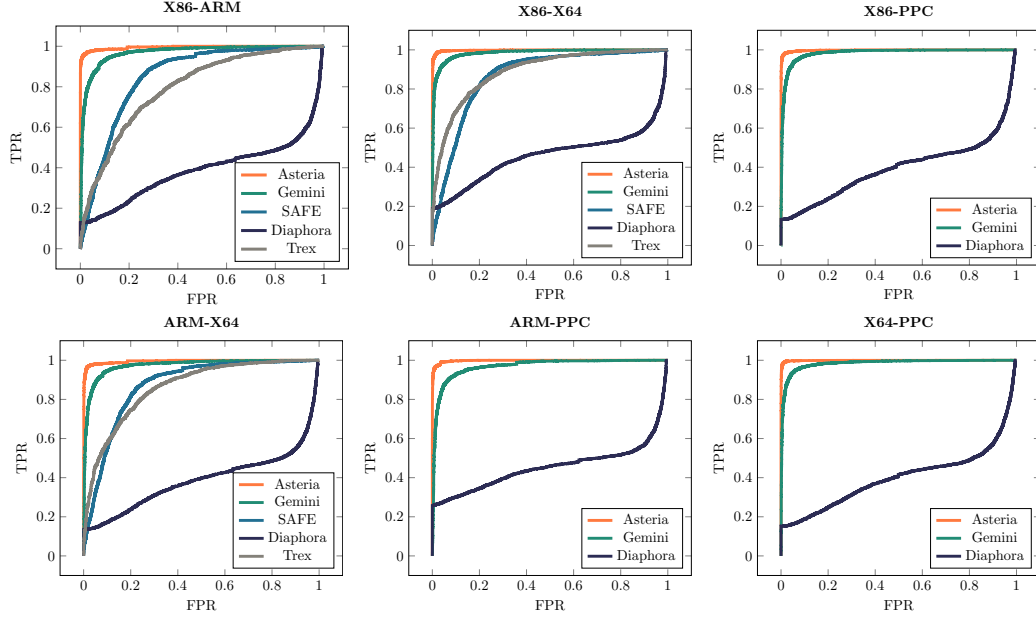


Fig. 9. ROC Curves on All Cross-architecture Combination Detection.

Table 3. MRR and Recall of Different Methods.

Metrics	Methods	X86-X64	X86-ARM	X86-PPC	X64-ARM	X64-PPC	ARM-PPC	Avg
MRR	ASTERIA-PRO	0.934	0.887	0.931	0.879	0.919	0.903	0.908
	Asteria	0.776	0.724	0.731	0.708	0.713	0.750	0.734
	Trex	0.414	0.206	-	0.309	-	-	0.310
	Gemini	0.478	0.250	0.325	0.336	0.357	0.256	0.334
	Safe	0.029	0.007	-	0.009	-	-	0.015
	Diaphora	0.023	0.019	0.020	0.019	0.020	0.021	0.020
Recall@Top-1	ASTERIA-PRO	0.917	0.868	0.912	0.879	0.899	0.903	0.896
	Asteria	0.706	0.648	0.652	0.627	0.631	0.675	0.657
	Trex	0.274	0.110	-	0.192	-	-	0.192
	Gemini	0.405	0.180	0.242	0.261	0.279	0.229	0.266
	Safe	0.004	0.002	-	0.002	-	-	0.003
	Diaphora	0.021	0.016	0.017	0.016	0.017	0.018	0.018
Recall@Top-10	ASTERIA-PRO	0.961	0.921	0.962	0.913	0.952	0.932	0.940
	Asteria	0.902	0.867	0.882	0.857	0.866	0.890	0.877
	Trex	0.710	0.452	-	0.575	-	-	0.579
	Gemini	0.615	0.383	0.482	0.478	0.502	0.468	0.488
	Safe	0.022	0.010	-	0.014	-	-	0.015
	Diaphora	0.029	0.024	0.026	0.026	0.025	0.027	0.026

Comparison on task-V. As shown in Table 3, we calculate MRR, Recall@Top-1, and Recall@Top-10 for a variety of architectural combinations. Recall@Top-1 is a rigorous metric that indicates the robust detection capacity of homologous functions, whereas Recall@Top-10 demonstrates the capability to rank homologous functions in the top ten positions. In the first column of the table are the metrics, and in the second column are the names of the methods. The third through eighth columns provide the metric values for the various architectural combinations, whereas the last column displays the mean for all architectures. **ASTERIA-PRO** and *Asteria* consistently outperform baseline approaches by a

```

1 CK_RV proxy_C_DigestInit(...){
2     /*
3      Variable Initialization.
4      */
5     v5 = (Proxy *)self[1].  

6         C_GetSlotInfo;  

7     v7 = handle;  

8     result = map_session_to_real(  

9         v5,&v7,&map,V3);  

10    if (!result)  

11        result = map.funcs->C_  

12            DigestInit(v7,  

13                mechanism);  

14    return result;  

15 }
```

```

1 CK_RV proxy_C_DigestKey(...){
2     /*
3      Variable Initialization.
4      */
5     v5 = (Proxy *)self[1].  

6         C_GetSlotInfo;  

7     v7 = handle;  

8     result = map_session_to_real(  

9         v5,&v7,&map,V3);  

10    if (!result)  

11        result = map.funcs->C_  

12            DigestKey(v7, mechanism  

13                );  

14    return result;  

15 }
```

Fig. 10. Two Proxy Functions with only distinctions highlighted in red

significant margin across all architecture configurations. **ASTERIA-PRO** achieves a very high average MRR (0.908), indicating an MRR improvement of up to 23.71% compared to *Asteria*. Even after retraining, *Safe*'s detection results demonstrate that it improperly recognizes small functions despite its poor performance. Regarding Recall@Top-1, **ASTERIA-PRO** and *Asteria* attain relatively high average precisions (0.89 and 0.65, respectively) that are 237% and 146% greater than the best result (0.26). **ASTERIA-PRO** has a 36.4% improvement in Recall@Top-1 vs *Asteria*. Regarding the metric Recall@Top-10, **ASTERIA-PRO** and *Asteria* continue to reign supreme. In comparison to Recall@Top-1, we observe that the recall of other methods, such as *Trex*, increases dramatically, from 0.192 to 0.579, indicating that they are able to rate homologous sequences quite highly. However, they are still far below **ASTERIA-PRO**.

Despite the similar ROC curve performance of *Asteria*, *Gemini*, *SAFE*, and *Trex*, their Task-V performance is entirely different. *Gemini*, for instance, has a large AUC score of 0.977, which is similar to *Asteria*'s 0.997. However, in terms of MRR, *Gemini* performs poorly (0.333) compared to *Asteria* (0.734) and **ASTERIA-PRO** (0.908). This suggests that testing BCSD approaches in a single experiment setting (such as the Task-C setting) is insufficient to demonstrate application behavior.

False Positive Analysis. There are two primary causes for *Asteria*'s false positive outcomes.

- **Cause 1.** Proxy functions hold similar syntactic structures, resulting in similar semantic. Figure 10 illustrates two proxy functions that differ solely on line 9. *Asteria-Pro* fails to differentiate proxy functions since their semantics are similar. In addition, the callees are difficult to confirm due to indirect jump table when symbols are lacking.
- **Cause 2.** Compilers for distinct architectures utilize various intrinsic functions that substitute libc function calls with optimized assembly instructions. For instance, the gcc-X86 compiler may replace the memcpy function with several memory operation instructions, causing the function to be absent from the callee function list. *Asteria*'s filtering and re-ranking modules lack a complete set of callee functions for score calculation, resulting in a loss of precision.

Answer to RQ1: **ASTERIA-PRO** demonstrates superior accuracy in both Task-C and Task-V. In Task-C, dominant model in **ASTERIA-PRO** demonstrates the best classification performance by producing the highest AUC (0.997). Regarding Task-V, **ASTERIA-PRO** outperforms other baseline methods by a large margin in MRR, Recall@Top-1, and Recall@Top-10. In particular, **ASTERIA-PRO** has 172%, 236%, 147% higher MRR, Recall@Top-1, Recall@Top-10 than the best baseline methods. Compared with Asteria, **ASTERIA-PRO** manages to improve it for Task-V with 23.71% higher MRR, 36.4% higher Recall@Top-1, and 7.2% higher Recall@Top-10.

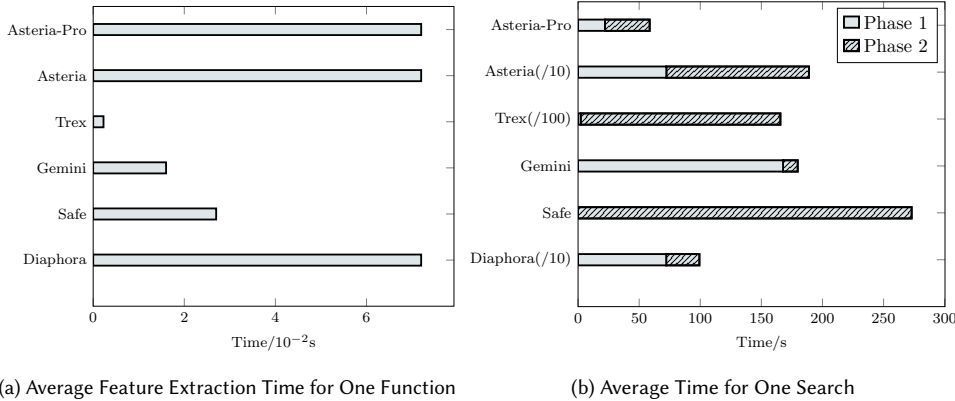


Fig. 11. Performance Comparison of All Methods on Task-V

8.6 Performance Comparison (RQ2)

In this section, the detection time of function similarity for all baseline approaches and **ASTERIA-PRO** are measured. Since the DK-based prefiltration and DK-based re-ranking modules are intended to enhance performance in Task-V, we only count the timings in Task-V. In task-V, given a source function, methods extract the function features of source and all candidate functions, which is referred to as *phase 1*. Next, the extracted function features are subjected to feature encoding and encoding similarity computation to determine the final similarities, which is referred to as *phase 2*.

As shown in Figure 11a, we calculate the average feature extraction time for each function. The x-axis depicts extraction time, while the y-axis lists various extraction methods. During phase 1, **ASTERIA-PRO**, Asteria, and Diaphora all execute the same operation (i.e., AST extraction), resulting in the same average extraction time. Since AST extraction requires binary disassembly and decompilation, it requires the most time compared to other methods. Trex requires the least amount of time for feature extraction, which is less than 0.001s per function, as code disassembly is the only time-consuming activity.

Figure 11b illustrates the average duration of a single search procedure for various methods. The phases 1 and 2 of a single search procedure are denoted by distinct signs. Due to its efficient filtering mechanism, **ASTERIA-PRO** requires the least amount of time (58.593s) to complete a search. Due to its extensive pre-training model encoding computation, Trex is the most time-consuming algorithm. **ASTERIA-PRO** cuts search time by 96.90%, or 1831.36 seconds, compared to Asteria (1889.96 seconds).

Answer to RQ2: ASTERIA-PRO costs the least average time to accomplish task-V. Compared with Asteria, **ASTERIA-PRO** cuts search time by 96.90% by introducing the filtering module.

Table 4. Accuracy of Different Module Combination

Module Combination	MRR	Recall@Top-1	Recall@Top-10	Average Time(s)
Pre-filtering + Asteria	0.824	0.764	0.929	57.8
Asteria + Reranking	0.882	0.864	0.910	1889.8

8.7 Ablation Experiments (RQ3)

To demonstrate the progresses made by different modules of DK-based filtration and DK-based re-ranking, we conduct ablation experiments by evaluating the different module combinations in **ASTERIA-PRO**. The module combinations are *Pre-filtering + Asteria* and *Asteria + Re-ranking*. The two module combinations performs Task-V and the results are shown in Table 4. For *Asteria + Re-ranking*, the top 20 similarity detection results are re-ranked by the Re-ranking module.

Filtration Improvement. Compared to Asteria, the integration of pre-filtering improves MRR, Recall@Top-1, and Recall@Top-10 by 12.26%, 16.29%, and 5.93%, respectively. In term of efficiency, it cuts search time by 96.94%. The *Pre-filtering + Asteria* combination performs better than *Asteria + Re-ranking* in terms of *Recall@Top-10* and time consumption. It generates a greater *Recall@Top-10* because it filters out a large proportion of highly rated non-homologous functions.

Re-ranking Improvement. Compared to Asteria, the integration of Re-ranking module improves MRR, Recall@Top-1, and Recall@Top-10 by 20.16%, 31.51%, and 3.76%, respectively. In terms of efficiency, it costs average additional 0.13s for re-ranking, which is negligible. Compared to *Pre-filtering + Asteria*, re-ranking module contributes to an increase in *MRR* and *Recall@Top-1* by enhancing the rank of homologous functions.

Answer to RQ3: The filtering significantly cuts the calculation time by 96.94%, and increase precision slightly. Re-ranking improves MRR, Recall@Top-1, and Recall@Top-10 by 20.16%, 31.51%, and 3.76%, respectively, with negligible time costs.

Table 5. Capacity to Filter of Various Filtering Thresholds.

T_{GL}	# Filtered Function	Recall
0.1	9666.7	0.9813
0.2	9734.1	0.9808
0.3	9777.4	0.9791
0.4	9793.5	0.9773
0.5	9805.5	0.9737

8.7.1 Different Filtering Threshold. In Algorithm 1, the threshold T_{GL} determines the number of functions that are filtered out. We evaluate the efficacy of the filtering module by utilizing various T_{GL} values, and the results are presented in Table 5. The threshold values range from 0.1 to 0.5 in the first column, where a higher threshold value suggests a more severe selection of the similarity function. The second column indicates the number of functions omitted by the filter, while the third column displays the recall rate in the filtration results. As the threshold value increases, the recall rate declines and the number of filtered-out functions grows. We use 0.1 as our threshold value for two key reasons: a) the high recall rate of filtering results is advantageous for subsequent homologous function detection, and b) there is no significant difference in the number of functions that are filtered out.

8.8 Real World Bug Search (RQ4)

To assess the efficacy of **ASTERIA-PRO**, we conduct a massive real-world search for bugs. To accomplish this, we obtain firmware and compile vulnerability functions to create a firmware dataset and a vulnerability dataset. Utilizing vulnerability dataset, we then apply **ASTERIA-PRO** to detect vulnerable functions in the firmware dataset. To confirm vulnerability in the resulting functions, we design a semi-automatic method for identifying vulnerable functions. Through a comprehensive analysis of the results, we discover intriguing facts regarding vulnerabilities existed in IoT firmware.

Table 6. Vulnerability Dataset

Software	CVE #	Disclosure Years	Vulnerable Version Range
OpenSSL	22	2013~2016	[1.0.0, 1.0.0s]
			[1.0.1, 1.0.1t]
			[1.0.2, 1.0.2h]
Busybox	10	2015~2019	[0.38, 1.29.3]
Dnsmasq	14	20{15,17,20,21}	[2.42, 2.82], 2.86
Lighttpd	10	20{08,10,11,13,14,15,18}	[1.3.11, 1.4.49]
Tcpdump	36	2017	[3.5.1, 4.9.1]

8.8.1 Dataset Construction. In contrast to our prior work, we expand both the vulnerability dataset and the firmware dataset for a comprehensive vulnerability detection evaluation.

Vulnerability Dataset. The prior vulnerability dataset of 7 CVE functions is enlarged to 90, as shown in Table 6. Vulnerability information is primarily gathered from the NVD website [11]. As shown in the first column, the vulnerabilities are collected from widely used open-source software in IoT firmware, including OpenSSL, Busybox, Dnsmasq, Lighttpd, and Tcpdump. In the second column, the number of software vulnerabilities is listed. In the third column, the timeframe or specific years of the disclosure of the vulnerability are listed. The final column describes the software version ranges affected by vulnerabilities. Note that the version ranges are obtained by calculating the union of all versions mentioned in the vulnerability reports. As a result, **ASTERIA-PRO** is expected to generate vulnerability detection results for all software versions falling within the specified ranges.

Firmware Dataset. We download as much of firmware from six popular IoT vendors as we could, consisting of Netgear [3], Tp-Link [14], Hikvision [10], Cisco [7], Schneider [13], and Dajiang [8] as shown in first column of Table 7. These firmware are utilized by routers, IP cameras, switches, and drones, all of which play essential parts in our life. The

Table 7. Firmware Dataset and Its Software Statistics. # denotes number.

Vendor	Firmware Dataset			Software Statistics				
	Firmware #	Binary #	Function #	OpenSSL	Busybox	Dnsmasq	Lighttpd	Tcpdump
Netgear	548	984	2,627,143	349	512	85	14	24
TP-Link	95	177	427,795	66	90	11	3	7
Hikvision	90	92	279,299	55	35	0	0	2
Cisco	29	66	60,396	23	26	10	5	2
Schneider	10	20	31,228	7	9	2	2	0
Dajiang	7	16	57,275	7	7	1	0	1
All	779	1,355	3,483,136	507	679	109	24	36

second column shows the firmware numbers, which range from 7 to 548. The third and fourth columns gives numbers of binaries and functions after unpacking firmware by using binwalk. Note that the binary number is the number of software selected to be in the vulnerability dataset. The fifth column to ninth column gives the five software numbers in all firmware vendors. OpenSSL and Busybox are widely integrated in these IoT firmware as their numbers are close to those of the firmware. Through querying their official websites for device type information, we find that the majority of Hikvision vendor firmware is for IP cameras, whereas Cisco vendor firmware is for routers. In particular, IP camera firmware incorporates less software than router firmware because routers offer more functionality. For example, the firmware of the Cisco RV340 router includes OpenSSL, Tcpdump, Busybox, and Dnsmasq, whereas the majority of IP camera firmware only include OpenSSL. Similarly, the majority of the firmware of Netgear and Tp-Link consists of routers, while Schneider and Dajiang'firmware include specialized devices such as Ethernet Radio and Stabilizers.

8.8.2 Large Scale Bug Search. **ASTERIA-PRO** is employed to identify vulnerable homologous functions among 3,483,136 firmware functions by referencing 90 functions from the vulnerability dataset. Specifically, in order to expedite the detection process, vulnerability detection is restricted to the same software between firmware dataset and vulnerability dataset. For instance, the vulnerable functions disclosed in OpenSSL are utilized to detect vulnerable homologous functions in OpenSSL in the firmware dataset. For each software S , we first extract features (i.e., ASTs and call graphs) of all functions in firmware dataset and vulnerable functions in vulnerability dataset. For each vulnerability disclosed in S , the pre-filtration module uses the call graph to filter out non-homologous functions, followed by the Tree-LSTM model encoding all remaining functions as vectors. **ASTERIA-PRO** then computes the AST similarity between the vulnerable function vectors and the firmawre function vector. **ASTERIA-PRO** computes reranking scores based on the top 20 of AST similarities based on similarity scores, since the evaluation demonstrates a very high recall in the top 20. As a final step, **ASTERIA-PRO** generates 20 candidate homologous functions for each S as a **bug search result** for each vulnerability. To further refine the bug search results, we compute the average similarity score of homologous functions in Section 8.5 and use it to eliminate non-vulnerable functions. In particular, the average similarity score of 0.89 is used to eliminate 3987 of 5604 results. We perform heuristic confirmation of vulnerability for the remaining 1617 results.

Vulnerability Confirmation Method. We devise a semi-automatic method for confirming the actual vulnerable functions from the candidate homologous functions. The method makes use of the symbols and string literals within the firmware binaries of the target. Specifically, we use unique regular expressions to match version strings for each software and to extract function symbols from the software. The method is then comprised of two distinct operations that correspond to two distinct vulnerable circumstances VC_1 , VC_2 .

- VC_1 . In this circumstances, the target binary contains version string (e.g., “OpenSSL 1.0.0a”) and the symbol of target function is not removed.
- VC_2 . Target binary contains version strings whereas the symbol of vulnerable homologous function is removed.

The versions of software listed in Table 6 are easy to extract using version strings [26]. The descriptions of the two confirmation operations CO_1 and CO_2 are as follows:

- CO_1 . For VC_1 , we confirm the vulnerable function based on the version and name of the target software. In particular, a vulnerable function is confirmed when the following two conditions are met: 1) software version is in vulnerable version range, 2) the vulnerable function name retains after elimination with average similarity score.
- CO_2 . For VC_2 , if the software versions are in the range of vulnerable versions, we manually compare the code between the CVE functions and remaining functions to confirm the vulnerability.

Table 8. Numbers of Vulnerable Functions, Software, Firmware in Confirmation Results.

vendor	Vulnerable Function #						Vulnerable Software #						Vulnerable Firmware #
	OpenSSL	Busybox	Dnsmasq	Lighttpd	Tcpdump	All	OpenSSL	Busybox	Dnsmasq	Lighttpd	Tcpdump	All	
Netgear	367	0	31	0	26	424	133	0	7	0	10	150	145 (26.46%)
TP-Link	394	9	0	2	5	410	36	3	0	2	5	46	36 (37.89%)
Hikvision	553	0	0	0	12	565	52	0	0	0	1	53	53 (58.89%)
Cisco	0	0	0	0	2	2	0	0	0	0	2	2	2 (6.90%)
Schneider	10	0	0	0	0	10	1	0	0	0	0	1	1 (10.00%)
Dajiang	70	0	0	0	1	71	7	0	0	0	0	8	7 (100.00%)
Total	1,394	9	31	2	46	1,482	229	3	7	2	19	260	244 (31.32%)

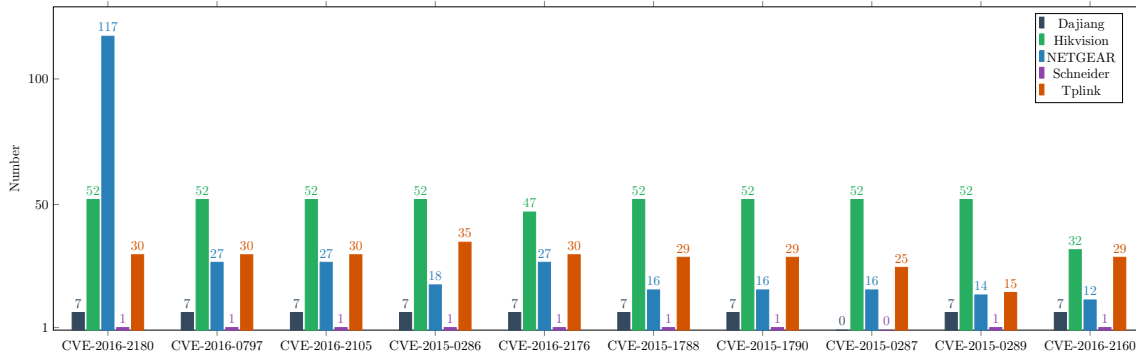


Fig. 12. # of Vulnerable Functions Detected from Five Vendors

Results Analysis. In Table 8, we tally the number of vulnerable functions, software, and firmware upon vulnerability confirmation. The first column contains the names of different vendors. The second through sixth columns show the amount of vulnerable functions in various software, while the seventh column indicates the total number of vulnerable functions across all vendors. The eighth through twelfth columns display the amount of vulnerable software binaries in various software, while the thirteenth column provides the total number of vulnerable software binaries. According to the seventh column of Table 7, there are a total of 1,482 vulnerable functions. 1456 are confirmed by VO_1 , whereas 26 are confirmed by VO_2 . For a total of 1,456 VO_1 vulnerable functions, 1,377 vulnerable functions rank first and 79

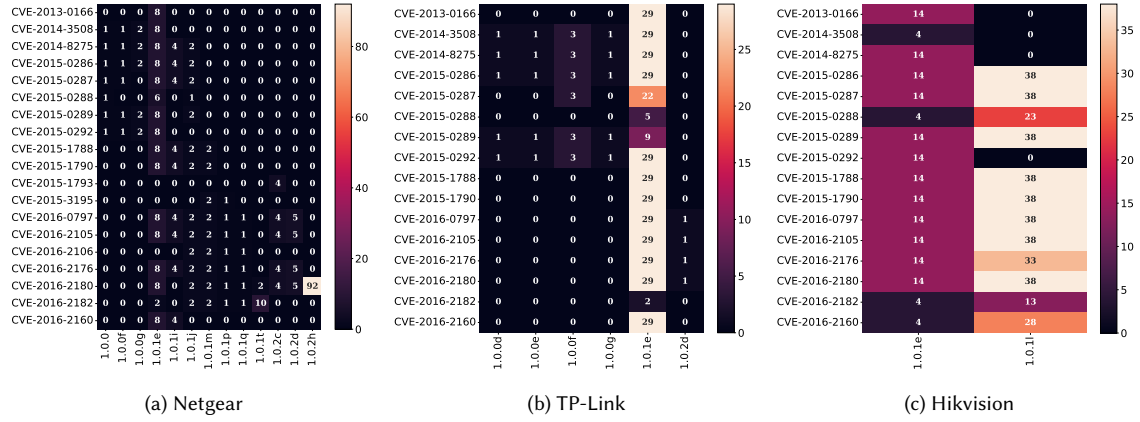


Fig. 13. The Distribution of CVEs for Different OpenSSL Versions in vendors Netgear, TP-Link, Hikvision from left to right.

vulnerable functions rank second. VO_2 is performed on 47 detection results, of which 26 are confirmed. Since they contain the majority of functions, three vendors, Netgear, Tp-Link, and Hikvision, account for the vast majority (94.4%) of vulnerable functions. Specifically, a large proportion of vulnerable functions are found in the OpenSSL software used by the three vendors. The number of vulnerable software is consistent with this circumstance. The final column shows the number of firmware containing at least one vulnerable function, together with its proportion of total firmware. Every *Dajiang* firmware contains at least one CVE vulnerability because all OpenSSL components used in firmware are vulnerable. In addition, Hikvision is detected to have a large proportion of vulnerable firmware (58.89%). To inspect the CVE vulnerable function distribution, we plot the top 10 CVEs and their distributions in five vendors except Cisco in Figure 12, since Cisco takes additional two CVEs.

- **Top 10 CVE Analysis.** Figure 12 demonstrates the top 10 CVE distribution in various vendors. The total number of discovered CVE vulnerabilities decreases from left to right along the x-axis. Except for CVE-2015-0287, all of the top 10 CVE vulnerabilities are discovered in every *Dajiang* firmware. This is because *Dajiang* utilizes an outdated version of OpenSSL 1.0.1h that contains numerous vulnerable functions [12]. Although Hikvision firmware has the third largest number of firmware, it has the most vulnerable functions in our experiment settings. The reason for this is that Hikvision firmware heavily uses OpenSSL-1.0.1e (184) and OpenSSL-1.0.1l (401) versions, both of which contain a large number of vulnerabilities. **Finding:** Since they typically adopt the same vulnerable software version, it is highly plausible that firmware from the same vendor and released at the same period contains identical vulnerabilities. Security analysts can quickly narrow down the vulnerability analysis based on the firmware release date.
- **CVE and Version Analysis.** Figure 13 depicts the distribution of vulnerable OpenSSL versions for various CVEs from various vendors. where the x-axis represents the version and the y-axis represents the CVE ID associated with the vulnerability. Each square in each subfigure indicates the number of OpenSSL versions that are vulnerable and contain the corresponding CVE along the y-axis. The number is greater the lighter the red colour. The left subfigure demonstrates that OpenSSL 1.0.2h is widely used by Netgear, resulting in a significant number of CVE-2016-2180 vulnerabilities (92). Additionally, OpenSSL version 1.0.1e exposes the majority of CVEs listed on the y-axis, which may increase the device's attack surface. The TP-Link firmware incorporates

OpenSSL version 1.0.1e, resulting in brighter hues. Hikvision firmware utilizes versions 1.0.1e and 1.0.1l, which are vulnerable to a number of CVEs. Comparing vulnerability distribution in OpenSSL version 1.0.1e among different vendors reveals inconsistencies in the existence of vulnerabilities. For instance, CVE-2016-2106 is present in OpenSSL 1.0.1e from Hikvision but not from Netgear and TP-Link. **Finding:** Despite using the same version of software, various vendor firmware behaves differently in terms of vulnerability since they can tailor the software to the device's specific capabilities.

- **CVE-2016-2180 Analysis.** The CVE-2016-2180, which is a remote *Denial-of-Service* flaw caused by received forged time-stamp file, impacting OpenSSL 1.0.1 through 1.0.2h, exists in 207 firmware. NETGEAR is responsible for 117 of these, as it deploys 92 OpenSSL 1.0.2h out of a total of 548 firmware. NETGEAR incorporated an extra nine OpenSSL 1.0.2 series software and sixteen OpenSSL 1.0.1 series software. The vulnerable version 1.0.2h was released in May 2016, and by comparing their timestamps, we determined that OpenSSL 1.0.2h was integrated into firmware between 2016 and 2019. **Finding:** Even after their vulnerabilities have been discovered, the vulnerable versions of software continue to be used for firmware development.

Based on the confirmation results, **ASTERIA-PRO** manages to detect 1,482 vulnerable functions out of 1617 bug search results, indicating that **ASTERIA-PRO** achieves a high vulnerability detection precision of **91.65%** under our experiment settings. By randomly selecting 1,000 of 5,604 bug search results, we manually validate the existence of vulnerabilities in software binaries in order to calculate the recall. Among 1000 bug search results, 205 target function are confirmed to be vulnerable by checking software versions and the vulnerable functions. Targeting 205 vulnerable functions, **ASTERIA-PRO** detects 53 of them, representing a recall rate of 25.85%.

Finding Inlined Vulnerable Code. During the analysis of mismatched cases, in which the target homologous functions are not in the top ranking position, we observe that the top-ranked functions contain the same vulnerable code. We use CVE-2017-13001 as an illustration of inlined vulnerable code detection. CVE-2017-13001 is a buffer over-read vulnerability in the Tcpdump *nfs_printf* function prior to version 4.9.2. After a confirmation operation CO_2 , **ASTERIA-PRO** reports a single function, *parsefh* as being vulnerable. We manually compare the decompiled code of the *parsefh* function to the source code of *nfs_printf* in tcpdump version 4.9.1 (i.e., vulnerable version). Figure 14 demonstrates that the source code of *nfs_printf* (on the left) and the partial code of *parsefh* (on the right) are consistent. We designate codes with apparently identical semantics with distinct backdrop hues. In other words, during compilation, function *nfs_printf* is inlined into function *parsefh*. As a result, the function *parsefh* contains CVE-2017-13001 vulnerable code, and **ASTERIA-PRO** manages to identify the inlined vulnerable code. **ASTERIA-PRO** has detected an additional eight instances of inlined vulnerable code out of 20 functions in vulnerable circumstance VC_2 .

The preceding analysis and conclusions are constrained by the dataset we constructed, which offers security analysts some recommendations for the security analysis of firmware.

Answer to RQ4. We employ 90 CVE vulnerabilities to search for bugs in 3,483,136 real firmware functions. **ASTERIA-PRO** detects 1,482 vulnerable functions with a high level of precision of 91.65%. In addition, the capability of **ASTERIA-PRO** to identify inlined vulnerable code is stated and illustrated in detail. In conclusion, **ASTERIA-PRO** generates bug search results with a high degree of confidence, thereby reducing analysis labor by a substantial margin.



Figure 14 consists of two side-by-side code snippets. The left snippet, labeled (a), is the source code of a vulnerable function. The right snippet, labeled (b), is a small portion of the decompiled code from a detected function. Both snippets use color-coded highlighting to group similar semantic code blocks. The snippets are as follows:

```

(a) Source Code of Vulnerable Function.
1  {
2  ...
3  if (ndo->ndo_uflag) {
4      u_int i;
5      char const *sep = "";
6      ND_PRINT((ndo, " fh["));
7      for (i=0; i<len; i++) {
8          ND_PRINT((ndo, "%s%x", sep, dp[i]));
9          sep = ":";  

10     }
11     ND_PRINT((ndo, "]"));
12     return;
13 }
14 Parse_fh((const u_char *)dp, len, &fsid, &ino,
15           NULL, &fsname, 0);
16 if (fsname) {
17     ...
18     strncpy(temp, fsname, strlen);
19     temp[strlen] = '0';
20     spacep = strchr(temp, ' ');
21     if (spacep)
22         *spacep = '0';
23     ND_PRINT((ndo, " fh %s/", temp));
24 } else {
25     ND_PRINT((ndo, " fh %d,%d",
26               fsid.Fsid_dev.Major, fsid.Fsid_dev.Minor));
27 }
28 if(fsid.Fsid_dev.Minor == 257)
29     ND_PRINT((ndo, "%s", fsid.Opaque_Handle));
30 else
31     ND_PRINT((ndo, "%ld", (long) ino));
32 }

```

```

(b) A Small Portion of Decompiled Code in Detected Function.
1  {
2  ...
3  if ( v8 )
4  {
5      printf(" fh[");
6      if ( v4 ){
7          for ( i = 0; i < v4; ++i ){
8              v11 = *(_DWORD *)&v3[4 * i];
9              printf("%s%x", v9, v11);
10             v9 = ":";  

11         }
12     }
13     putchar(93);
14     return &v3[v5];
15 }else{
16     Parse_fh(v3, v4, v13, &v16, 0, &src, 0);
17     if ( src){
18         strncpy(temp_5711, src, 0x40u);
19         byte_B9E04 = 0;
20         v12 = strchr(temp_5711, 32);
21         if ( v12 )
22             *v12 = 0;
23         printf(" fh %s/", temp_5711);
24     }else{
25         printf(" fh %d,%d/", v13[1], v13[0]);
26     }
27     if ( v13[0] == 257 )
28         printf("%s", v14);
29     else
30         printf("%ld", v16);
31     return &v3[v5];
32 }

```

(a) Source Code of Vulnerable Function.

(b) A Small Portion of Decompiled Code in Detected Function.

Fig. 14. Inlined Vulnerable Function in Detected Function. The semantics of the code with the same background color are same.

9 THREATS TO VALIDATION.

Threats to internal validity come from these aspects.

- We use vulnerable version ranges collected from the NVD website to aid vulnerability confirmation in a real-world bug-search experiment. The vulnerable version ranges may be inaccurate, and vulnerabilities may be missed or incorrectly stated. We will conduct additional verification of the susceptible version ranges by confirming the existence of vulnerable code.
- We adopt IDA Pro to decompiling and generate ASTs from the functions in binaries. As pointed by study [46], accurate decompiling and binary analysis is not easy. The errors in AST generation may affect the AST similarity calculation and further affect the results.

Threats to external validity rise from following issue.

- In practice, firmware binaries may be compiled with distinct compiler (e.g., clang), compiler version, and optimization level for special-purpose compilation. Different compilation configurations alter the AST structures and call graphs, sometimes leading in lower scores for homologous functions.

10 RELATED WORKS

Feature-based Methods. When considering the similarity of binary functions, the most intuitive way is to utilize the assembly code content to calculate the edit distance for similarity detection between functions. Khoo *et al.* concatenated consecutive mnemonics from assembly language into the N-grams for similarity calculation [43]. David *et al.* proposed Trecelet, which concatenates the instructions from adjacent basic blocks in CFGs for similarity calculation [23]. Saebjornsen *et al.* proposed to normalize/abstract the operands in instructions, e.g., replacing registers such as eax or ebx with string “reg”, and conduct edit distance calculation based on normalized instructions [55]. However, binary code similarity detection methods based on disassembly text can not be applied to cross-architecture detection since the instructions are typically different in different architectures. The works in [54], [18], [30], [65] utilize cross-architecture statistical features for binary code similarity detection. Eschweiler *et al.* [30] defined statistical features of functions such as the number of instructions, size of local variables. They utilized these features to calculate and filter out candidate functions. Then they performed a more accurate but time-consuming calculation with the graph isomorphism algorithm based on CFGs. Although this method takes a pre-filtering mechanism, the graph isomorphism algorithm makes similarity calculation extremely slow. To improve the computation efficiency, Feng *et al.* proposed Genius which utilizes machine learning techniques for function encoding [32]. Genius uses the statistical features of the CFG proposed in [30] to compose the attributed CFG (ACFG). Then it uses a clustering algorithm to calculate the center points of ACFGs and forms a codebook with the center points. Finally, a new ACFG is encoded into a vector by computing the distance with ACFGs in the codebook and the similarity between ACFGs is calculated based on the encoded vectors. But the codebook calculation and ACFG encoding in Genius are still inefficient. Xu *et al.* proposed *Gemini* based on Genius to encode ACFG with a graph embedding network [64] for improving the accuracy and efficiency. However, the large variance of binary code across different architectures makes it difficult to find architecture-independent features [25].

Semantic-based Methods. For more accurate detection, semantic-based features are proposed and applied for code similarity detection. The semantic-based features model the code functionality, and are not influenced by different architectures. Khoo *et al.* applied symbolic execution technique for detecting function similarity [48]. Specifically, they obtained input and output pairs by executing basic blocks of a function. But the input and output pairs can not model the functionality of the whole function accurately. Ming *et al.* leveraged the deep taint and automatic input generation to find semantic differences in inter-procedural control flows for function similarity detection [52]. Feng *et al.* proposed to extract conditional formulas as higher-level semantic features from the raw binary code to conduct the binary code similarity detection [31]. In their work, the binary code is lifted into a platform-independent intermediate representation (IR), and the data-flow analysis is conducted to construct formulas from IR. Egele *et al.* proposed the blanket execution, a novel dynamic equivalence testing primitive that achieves complete coverage by overwriting the intended program logic to perform the function similarity detection [29]. These semantic-based features capture semantic functionalities of a function to reduce the false positives. Pei *et al.* proposes Trex [53], applying a transfer-learning-based framework to automate learning execution semantics from functions’ micro-traces, which are forms of under-constrained dynamic traces. However, the methods above depend heavily on emulation or symbolic execution, which are not suitable for

program analysis in large-scale IoT firmware since the emulation requires peripheral devices [19, 34, 70] and symbolic execution suffers from the problems of path explosion.

AST in Source Code Analysis. Since the AST can be easily generated from source code, there has been research work proposed to detect source code clone based on AST. Ira D. Baxter *et al.* proposed to hash ASTs of functions to buckets and compare the ASTs in the same bucket [16] to find clones. Because the method proposed in [16] is similar to *Diaphora* which hash ASTs, we only perform a comparative evaluation with *Diaphora*. In addition to the code clone detection, AST is also used in vulnerability extrapolation from source code [66, 67]. In order to find vulnerable codes that share a similar pattern, Fabian *et al.* [67] encoded AST into a vector and utilized the latent semantic analysis [24] to decompose the vector to multiple structural pattern vectors and compute the similarity between these pattern vectors. Yusuke Shido *et al.* proposed an automatic source code summary method with extended Tree-LSTM [57].

11 CONCLUSION

In this work, we present **ASTERIA-PRO**, a domain knowledge-enhanced BCSD tool designed to detect homologous vulnerable functions on a broad scale in efficient and accurate manner. **ASTERIA-PRO** introduces domain knowledge before and after deep learning model-based function encoding to eliminate a large proportion of non-homologous functions and score homologous functions higher, separately. The pre-filtering module makes extensive use of function name information prior to function encoding to accelerate the function encoding. The function call structure is utilized by the re-ranking module following function encoding to calibrate the encoding similarity scores. **ASTERIA-PRO** is capable of finding homologous functions rapidly and precisely, according to a comprehensive comparison with existing state-of-the-art research. Furthermore, **ASTERIA-PRO** manages to find 1,482 vulnerable functions in the real-world firmware bug search experiment with high precision of 91.65%. The search results for CVE-2017-13001 demonstrate **ASTERIA-PRO** successfully finds inlined vulnerable code. **ASTERIA-PRO** can aid in detecting vulnerabilities from large-scale firmware binaries to mitigate the attach damage on IoT devices.

REFERENCES

- [1] Buildroot making embedded linux easy. <https://buildroot.org>. [Online; accessed 26-February-2020].
- [2] Diaphora. <https://github.com/joxeankoret/diaphora>. Accessed jan 4, 2020.
- [3] Netgear download. <http://support.netgear.cn/download.asp>. [Online; Accessed May 19, 2020].
- [4] IDA Pro. <https://www.hex-rays.com/products/ida/index.shtml>, 2019. [Online; accessed 3-April-2020].
- [5] Binwalk. <https://www.refirmlabs.com/binwalk/>, 2020. [Online; accessed 5-April-2020].
- [6] Asteria-pro code repository. <https://github.com/Asteria-BCSD/Asteria-Pro>, 2022. [Online;].
- [7] Cisco website. https://www.cisco.com/c/en_hk/index.html, 2022. [Online;].
- [8] Dajiang website. <https://www.dji.com/>, 2022. [Online;].
- [9] function decoration. https://en.wikibooks.org/wiki/X86_Disassembly/Calling_Conventions#Note_on_Name_Decorations, 2022. [Online;].
- [10] hikvision website. <https://www.hikvision.com/sg/>, 2022. [Online;].
- [11] National vulnerability database. <https://nvd.nist.gov/>, 2022. [Online;].
- [12] Openssh 1.0.1h vulnerability statistics. <https://www.cvedetails.com/version/524410/Openssl-Openssl-1.0.1h.html>, 2022. [Online;].
- [13] schneider website. <https://www.se.com/ww/en/>, 2022. [Online;].
- [14] Tp-link website. <https://www.tp-link.com/sg/>, 2022. [Online;].
- [15] Hamid Abdul Basit and Stan Jarzabek. Detecting higher-level similarity patterns in programs. *SIGSOFT Softw. Eng. Notes*, 30(5):156–165, September 2005.
- [16] Ira D Baxter, Andrew Yahin, Leonardo Moura, Marcelo Sant’Anna, and Lorraine Bier. Clone detection using abstract syntax trees. In *Proceedings. International Conference on Software Maintenance (Cat. No. 98CB36272)*, pages 368–377. IEEE, 1998.
- [17] Chris Bogart, Christian Kästner, James Herbsleb, and Ferdian Thung. When and how to make breaking changes: Policies and practices in 18 open source software ecosystems. *ACM Transactions on Software Engineering and Methodology (TOSEM)*, 30(4):1–56, 2021.

- [18] Mahinthan Chandramohan, Yinxing Xue, Zhengzi Xu, Yang Liu, Chia Yuan Cho, and Hee Beng Kuan Tan. Bingo: Cross-architecture cross-os binary search. In *Proceedings of the 2016 24th ACM SIGSOFT International Symposium on Foundations of Software Engineering*, pages 678–689. ACM, 2016.
- [19] Daming D Chen, Maverick Woo, David Brumley, and Manuel Egele. Towards automated dynamic analysis for linux-based embedded firmware. 2016.
- [20] Cristina Cifuentes and K John Gough. Decompilation of binary programs. *Software: Practice and Experience*, 25(7):811–829, 1995.
- [21] Ang Cui, Michael Costello, and Salvatore Stolfo. When firmware modifications attack: A case study of embedded exploitation. 2013.
- [22] Yaniv David, Nimrod Partush, and Eran Yahav. Firmup: Precise static detection of common vulnerabilities in firmware. *ACM SIGPLAN Notices*, 53(2):392–404, 2018.
- [23] Yaniv David and Eran Yahav. Tracelet-based code search in executables. In *Proceedings of the 35th ACM SIGPLAN Conference on Programming Language Design and Implementation*, PLDI ’14, pages 349–360, New York, NY, USA, 2014. ACM.
- [24] Scott Deerwester, Susan T Dumais, George W Furnas, Thomas K Landauer, and Richard Harshman. Indexing by latent semantic analysis. *Journal of the American society for information science*, 41(6):391–407, 1990.
- [25] Vijay D’Silva, Mathias Payer, and Dawn Song. The correctness-security gap in compiler optimization. In *2015 IEEE Security and Privacy Workshops*, pages 73–87. IEEE, 2015.
- [26] Ruian Duan, Ashish Bijlani, Meng Xu, Taesoo Kim, and Wenke Lee. Identifying open-source license violation and 1-day security risk at large scale. In *Proceedings of the 2017 ACM SIGSAC Conference on computer and communications security*, pages 2169–2185, 2017.
- [27] Thomas Dullien and Rolf Rolles. Graph-based comparison of executable objects (english version). *SSTIC*, 5(1):3, 2005.
- [28] Manuel Egele, Maverick Woo, Peter Chapman, and David Brumley. Blanket execution: Dynamic similarity testing for program binaries and components. In *23rd {USENIX} Security Symposium ({USENIX} Security 14)*, pages 303–317, 2014.
- [29] Manuel Egele, Maverick Woo, Peter Chapman, and David Brumley. Blanket execution: Dynamic similarity testing for program binaries and components. In *23rd USENIX Security Symposium (USENIX Security 14)*, pages 303–317, San Diego, CA, 2014. USENIX Association.
- [30] Sebastian Eschweiler, Khaled Yakdan, and Elmar Gerhards-Padilla. discovre: Efficient cross-architecture identification of bugs in binary code. In *NDSS*, 2016.
- [31] Qian Feng, Minghua Wang, Mu Zhang, Rundong Zhou, Andrew Henderson, and Heng Yin. Extracting conditional formulas for cross-platform bug search. In *Proceedings of the 2017 ACM on Asia Conference on Computer and Communications Security*, pages 346–359, 2017.
- [32] Qian Feng, Rundong Zhou, Chengcheng Xu, Yao Cheng, Brian Testa, and Heng Yin. Scalable graph-based bug search for firmware images. In *Proceedings of the 2016 ACM SIGSAC Conference on Computer and Communications Security*, pages 480–491. ACM, 2016.
- [33] Debin Gao, Michael K Reiter, and Dawn Song. Binhunt: Automatically finding semantic differences in binary programs. In *International Conference on Information and Communications Security*, pages 238–255. Springer, 2008.
- [34] Eric Gustafson, Marius Muench, Chad Spensky, Nilo Redini, Aravind Machiry, Yanick Fratantonio, Davide Balzarotti, Aurelien Francillon, Yung Ryn Choe, Christopher Kruegel, et al. Toward the analysis of embedded firmware through automated re-hosting. pages 135–150, 2019.
- [35] Irfan Ul Haq and Juan Caballero. A survey of binary code similarity. *ACM Computing Surveys (CSUR)*, 54(3):1–38, 2021.
- [36] Laune C Harris and Barton P Miller. Practical analysis of stripped binary code. *ACM SIGARCH Computer Architecture News*, 33(5):63–68, 2005.
- [37] Anfeng He, Chong Luo, Xinmei Tian, and Wenjun Zeng. A twofold siamese network for real-time object tracking. In *Proceedings of the IEEE conference on computer vision and pattern recognition*, pages 4834–4843, 2018.
- [38] John L Hennessy and David A Patterson. *Computer architecture: a quantitative approach*. Elsevier, 2011.
- [39] Sepp Hochreiter and Jürgen Schmidhuber. Long short-term memory. *Neural Computation*, 9(8):1735–1780.
- [40] Roger A Horn. The hadamard product. In *Proc. Symp. Appl. Math*, volume 40, pages 87–169, 1990.
- [41] Xin Hu, Tzi-cker Chiueh, and Kang G Shin. Large-scale malware indexing using function-call graphs. In *Proceedings of the 16th ACM conference on Computer and communications security*, pages 611–620, 2009.
- [42] Xin Hu, Kang G Shin, Sandeep Bhatkar, and Kent Griffin. Mutantx-s: Scalable malware clustering based on static features. In *Presented as part of the 2013 {USENIX} Annual Technical Conference ({USENIX} {ATC} 13)*, pages 187–198, 2013.
- [43] Wei Ming Khoo, Alan Mycroft, and Ross Anderson. Rendezvous: A search engine for binary code. In *Proceedings of the 10th Working Conference on Mining Software Repositories*, pages 329–338. IEEE Press, 2013.
- [44] Amanda Lee and Travis Atkison. A comparison of fuzzy hashes: evaluation, guidelines, and future suggestions. In *Proceedings of the SouthEast Conference*, pages 18–25, 2017.
- [45] Bingchang Liu, Wei Huo, Chao Zhang, Wenchao Li, Feng Li, Aihua Piao, and Wei Zou. α diff: cross-version binary code similarity detection with dnn. In *Proceedings of the 33rd ACM/IEEE International Conference on Automated Software Engineering*, pages 667–678. ACM, 2018.
- [46] Zhibo Liu and Shuai Wang. How far we have come: testing decompilation correctness of c decompilers. In *Proceedings of the 29th ACM SIGSOFT International Symposium on Software Testing and Analysis*, pages 475–487, 2020.
- [47] Lannan Luo, Jiang Ming, Dinghao Wu, Peng Liu, and Sencun Zhu. Semantics-based obfuscation-resilient binary code similarity comparison with applications to software plagiarism detection. In *Proceedings of the 22nd ACM SIGSOFT International Symposium on Foundations of Software Engineering*, pages 389–400, 2014.
- [48] Lannan Luo, Jiang Ming, Dinghao Wu, Peng Liu, and Sencun Zhu. Semantics-based obfuscation-resilient binary code similarity comparison with applications to software plagiarism detection. In *ACM SIGSOFT International Symposium on Foundations of Software Engineering*, FSE 2014, pages 389–400, New York, NY, USA, 2014. ACM.

- [49] Andrea Marcelli, Mariano Graziano, Xabier Ugarte-Pedrero, Yanick Fratantonio, Mohamad Mansouri, and Davide Balzarotti. How machine learning is solving the binary function similarity problem. In *31st USENIX Security Symposium (USENIX Security 22)*, pages 2099–2116, Boston, MA, August 2022. USENIX Association.
- [50] Andrea Marcelli, Mariano Graziano, Xabier Ugarte-Pedrero, Yanick Fratantonio, Mohamad Mansouri, and Davide Balzarotti. How machine learning is solving the binary function similarity problem. In *31st USENIX Security Symposium (USENIX Security 22)*, pages 2099–2116, 2022.
- [51] Luca Massarelli, Giuseppe Antonio Di Luna, Fabio Petroni, Roberto Baldoni, and Leonardo Querzoni. Safe: Self-attentive function embeddings for binary similarity. In *International Conference on Detection of Intrusions and Malware, and Vulnerability Assessment*, pages 309–329. Springer, 2019.
- [52] Jiang Ming, Meng Pan, and Debin Gao. ibinhunt: Binary hunting with inter-procedural control flow. In *International Conference on Information Security and Cryptology*, pages 92–109. Springer, 2012.
- [53] Kexin Pei, Zhou Xuan, Junfeng Yang, Suman Jana, and Baishakhi Ray. Trex: Learning execution semantics from micro-traces for binary similarity. *CoRR*, abs/2012.08680, 2020.
- [54] Jannik Pewny, Behrad Garmany, Robert Gawlik, Christian Rossow, and Thorsten Holz. Cross-architecture bug search in binary executables. In *2015 IEEE Symposium on Security and Privacy*, pages 709–724. IEEE, 2015.
- [55] Andreas Sæbjørnsen, Jeremiah Willcock, Thomas Panas, Daniel Quinlan, and Zhendong Su. Detecting code clones in binary executables. In *Proceedings of the Eighteenth International Symposium on Software Testing and Analysis, ISSTA '09*, pages 117–128, New York, NY, USA, 2009. ACM.
- [56] Andrew Schulman. Finding binary clones with opstrings function digests: Part iii. *Dr. Dobb's Journal*, 30(9):64, 2005.
- [57] Yusuke Shido, Yasuaki Kobayashi, Akihiro Yamamoto, Atsushi Miyamoto, and Tadayuki Matsumura. Automatic source code summarization with extended tree-lstm. In *2019 International Joint Conference on Neural Networks (IJCNN)*, pages 1–8. IEEE, 2019.
- [58] Kai Sheng Tai, Richard Socher, and Christopher D Manning. Improved semantic representations from tree-structured long short-term memory networks. *arXiv preprint arXiv:1503.00075*, 2015.
- [59] Kai Sheng Tai, Richard Socher, and Christopher D. Manning. Improved semantic representations from tree-structured long short-term memory networks. *CoRR*, abs/1503.00075, 2015.
- [60] Hao Wang, Wenjie Qu, Gilad Katz, Wenyu Zhu, Zeyu Gao, Han Qiu, Jianwei Zhuge, and Chao Zhang. jtrans: jump-aware transformer for binary code similarity detection. In *Proceedings of the 31st ACM SIGSOFT International Symposium on Software Testing and Analysis*, pages 1–13, 2022.
- [61] Zheng Wang, Ken Pierce, and Scott McFarling. Bmat-a binary matching tool for stale profile propagation. *The Journal of Instruction-Level Parallelism*, 2:1–20, 2000.
- [62] Seunghoon Woo, Dongwook Lee, Sunghan Park, Heejo Lee, and Sven Dietrich. {V0Finder}: Discovering the correct origin of publicly reported software vulnerabilities. In *30th USENIX Security Symposium (USENIX Security 21)*, pages 3041–3058, 2021.
- [63] J. Wurm, K. Hoang, O. Arias, A. Sadeghi, and Y. Jin. Security analysis on consumer and industrial iot devices. In *2016 21st Asia and South Pacific Design Automation Conference (ASP-DAC)*, pages 519–524, 2016.
- [64] Xiaojun Xu, Chang Liu, Qian Feng, Heng Yin, Le Song, and Dawn Song. Neural network-based graph embedding for cross-platform binary code similarity detection. In *Proceedings of the 2017 ACM SIGSAC Conference on Computer and Communications Security*, pages 363–376. ACM, 2017.
- [65] Yinxing Xue, Zhengzi Xu, Mahinthan Chandramohan, and Yang Liu. Accurate and scalable cross-architecture cross-os binary code search with emulation. *IEEE Transactions on Software Engineering*, 45(11):1125–1149, 2018.
- [66] Fabian Yamaguchi, Felix Lindner, and Konrad Rieck. Vulnerability extrapolation: Assisted discovery of vulnerabilities using machine learning. In *Proceedings of the 5th USENIX conference on Offensive technologies*, pages 13–13, 2011.
- [67] Fabian Yamaguchi, Markus Lottmann, and Konrad Rieck. Generalized vulnerability extrapolation using abstract syntax trees. In *Proceedings of the 28th Annual Computer Security Applications Conference*, pages 359–368, 2012.
- [68] Shouguo Yang, Long Cheng, Yicheng Zeng, Zhe Lang, Hongsong Zhu, and Zhiqiang Shi. Asteria: Deep learning-based ast-encoding for cross-platform binary code similarity detection. In *2021 51st Annual IEEE/IFIP International Conference on Dependable Systems and Networks (DSN)*, pages 224–236. IEEE, 2021.
- [69] Wenzheng Yin, Katharina Kann, Mo Yu, and Hinrich Schütze. Comparative study of cnn and rnns for natural language processing. *arXiv preprint arXiv:1702.01923*, 2017.
- [70] Jonas Zaddach, Luca Bruno, Aurelien Francillon, Davide Balzarotti, et al. Avatar: A framework to support dynamic security analysis of embedded systems' firmwares. In *NDSS*, pages 1–16, 2014.
- [71] Mark H Zweig and Gregory Campbell. Receiver-operating characteristic (roc) plots: a fundamental evaluation tool in clinical medicine. *Clinical chemistry*, 39(4):561–577, 1993.